STUDY ON THE RELATIONSHIP BETWEEN PROCESS PLAN AND RESOURCE REQUIREMENT IN ADDITIVE MANUFACTURING

A Thesis
Submitted to the Graduate Faculty
of the
North Dakota State University
of Agriculture and Applied Science

By

AMM Nazmul Ahsan

In Partial Fulfillment of the Requirements
for the Degree of
MASTER OF SCIENCE

Major Department:
Industrial and Manufacturing Engineering

December 2017

Fargo, North Dakota

North Dakota State University
Graduate School

Title

STUDY ON THE RELATIONSHIP BETWEEN PROCESS PLAN AND RESOURCE REQUIREMENT IN ADDITIVE MANUFACTURING

By

AMM Nazmul Ahsan

The Supervisory Committee certifies that this ***disquisition*** complies with North Dakota State University's regulations and meets the accepted standards for the degree of

MASTER OF SCIENCE

SUPERVISORY COMMITTEE:

Dr. Bashir Khoda
Chair

Dr. Chrysafis Vogiatzis

Dr. Zhibin Lin

Approved:

01/02/2018
Date

Dr. Om Prakash Yadav
Department Chair

ABSTRACT

Resource consumption in additive manufacturing (AM) is often tied with the physical attribute of the fabricated part. Thus, optimizing the processes plan for minimum part fabrication resource requirement is a matter of great interest. In this thesis, the hierarchical nature of the AM process plan steps are emphasized and both build direction and material deposition direction are optimized while considering the resource requirement. A novel combined two-step optimization methodology is presented to determine optimal build direction for the object and material deposition direction for layers while considering minimum contour plurality, surface quality, build height, fabrication factor, and layer contour concavity to compensate for the fabrication and resource limitations. Furthermore, a concurrent process plan optimization methodology is presented focusing on fabrication complexity resulting from part geometry. Implementation of the proposed methodologies on several example parts indicates substantial reduction of their total build time.

ACKNOWLEDGEMENTS

I would like to express my sincere gratitude to my advisor Dr. Bashir Khoda for the invaluable guidance, support, and training he provided throughout this research. It's been a privilege for me to work in his lab under his guidance.

I am very grateful to Dr. Chrysafis Vogiatzis for invaluable instructions, sharing knowledge on optimization, being my committee member, and reviewing this thesis.

I want to sincerely thank Dr. Zhibin Lin for being my committee member, and providing valuable advice, insights, and reviewing this thesis.

Thanks to my lab colleague Md Ahasan Habib for being supportive and collaborative in accomplishing various tasks of this thesis.

Finally, I express my deepest gratitude to my mother and father for continual support, love, encouragement, sacrifice, and all the opportunities one can desire for.

DEDICATION

To my parents

TABLE OF CONTENTS

LIST OF TABLES

LIST OF FIGURES

1. INTRODUCTION

Additive Manufacturing (AM) processes are at the core of next generation manufacturing which focuses on accelerating the domestic manufacturing competitiveness and reviving the overall economy. Hailed as the "third industrial revolution" [26], AM has inverted the 'Design for Manufacturing' concept into 'Manufacture for Design.' The fundamental agility in AM processes comes with the layer based building technique from the digitized model. The digital object model is usually constructed using the CAD modeler or reverse engineering techniques. The validated model needs to be sliced with a set of intersecting parallel planes perpendicular to a predetermined build direction along which the layers are placed one upon another. Thus, the 3D model is discretized into a set of closed 2D slice contours generated from the intersection between the 3D geometric model of the object and the planes. Material is added within these sliced contours by following a specific tool path and the object is built by putting those consecutively.

Considering the desired attributes in the process and the object geometry, the process planning steps can be dramatically simplified in the layer-based manufacturing approach which can vary the resource requirements such as time and travel length. Such attributes include number of layers, shape and their size, single or multiple contour in a slice, support material, functionality, accuracy, and surface quality [9]. Each of these attributes depends upon the execution of the process steps and is often related with multiple process steps. As a result, the effect of these attributes is carried out between steps towards the finished object. Each of the AM process steps are equally important and can have significant impact on the attributes of the manufactured part. But due to their hierarchical relationship, predecessor process steps have more influence on the finished product than their successors. Figure 1 shows the hierarchical

process planning steps to fabricate an object with additive manufacturing techniques. The hierarchical steps can be distinguished as virtual and physical strategy.

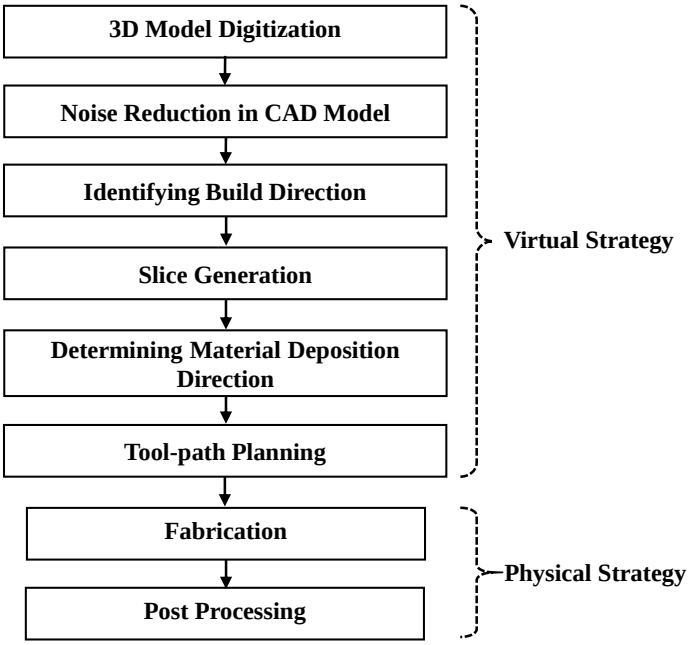

Figure 1. Hierarchical process plan for additive manufacturing.

1.1. Significance of the Work

Part attributes such as surface quality [1-15], accuracy [16], volumetric errors [17-20], support volume [2, 6, 21], and build time [2, 3, 5, 8-12, 15-17] are often used as metrics to optimize both virtual and physical strategies in process planning steps. However, with rapid growth and diversity in the technology, the weightage and effect of these matrices become dynamic and cannot be measured in a same scale. For an example, slicing an object along a predefined build direction creates closed contour called layer. For free-form shaped object with concave surface, multiple closed contours may be generated for the same layer in a particular build direction. Such phenomenon can be defined as contour plurality. Continuous material deposition gets disrupted for layers with contour plurality and generates tool start-stops as well as higher non-deposition time within layers. Such deposition disruption requires

machine/deposition system having very low response time, and high precision and resolution which in other word mean more resources. Careful selection of build orientation/direction of an object can significantly reduce the number of layers containing contour plurality. For instance, the first build orientation of the object shown in Figure 2(a) causes approximately 33% of the total number of layers to have four contours each as shown in Figure 2(b). Conversely, the second orientation of the same object shown in Figure 2(c) substantially reduces the amount of contour plurality as depicted in Figure 2(d).

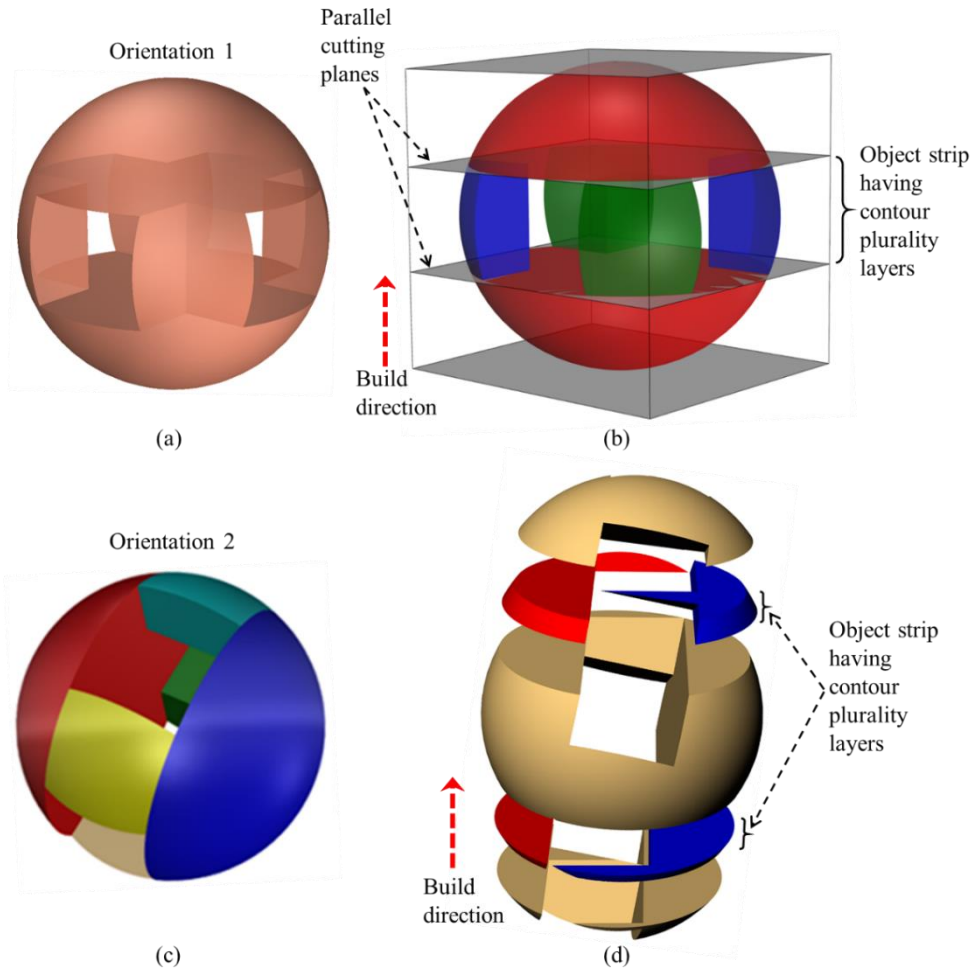

Figure 2. Change in the amount of contour plurality layers for two different build orientation/direction.

Furthermore, when the concave object surface is sliced, the resulting contour may contain consecutive upward (minima) or downward (maxima) segments which can be defined as contour concavity (see Figure 3). Continuous deposition will also be hampered because of tool start-stops along the area of concavity. However, clever choice of toolpath direction/orientation can also substantially reduce such non-value added machine activity (see Figure 3(b-c)).

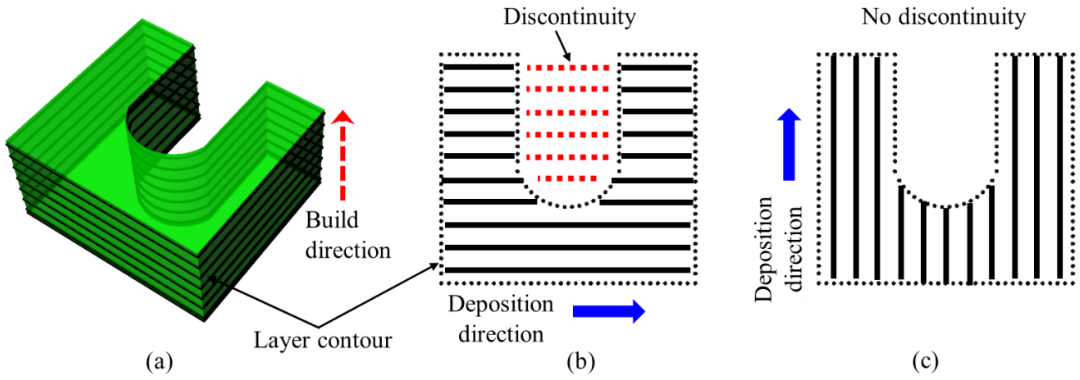

Figure 3. Contour concavity and deposition discontinuity.

Overall, discontinuity in material deposition/cure significantly increases the fabrication resource consumption in terms of machine hour and energy. However, very few efforts focusing on deposition continuity such as curve slicing [27] for fiber continuity and computational model [28] of continuous path planning for complex internal architecture have been reported in literature. Moreover, contour plurality and toolpath concavity have been frequently overlooked while determining the build direction as well as tool path in AM process plan. The presence of contour plurality in layers and concavity in the contour may increase build time and the discontinuity in the filament and may lower the structural integrity [29]. In this thesis, a systematic process plan frame work is presented for virtual strategies to minimize the resource consumption during part fabrication with AM techniques. Among the virtual strategies, build direction/orientation and material deposition direction steps are specially considered and the feature characteristics that are tied with them are identified in this work.

1.2. Objectives

This thesis represents a framework to determine resource based optimal process plan for virtual strategies of additive manufacturing process. The specific objectives of this research are as follows:

- Analyze object geometry and quantify contour plurality and contour concavity.
- Determine optimal part build direction/orientation for additive manufacturing techniques considering contour plurality, build height, part surface quality, and part geometric features.
- Determine optimal material deposition/toolpath direction considering contour concavity and toolpath discontinuity.
- Concurrently determine both part build direction and toolpath direction to minimize fabrication complexity of AM parts.

1.3. Overview of the Research

This thesis is organized as follows: Section 2 represents the background and review of literature on the virtual strategies of interest of AM processes. By incorporating the resource requirements with the generated object feature characteristics, a sequentially process plan optimization is proposed in this work. The workflow (1) of this modeling and optimization methodology is demonstrated in Figure 4. Section 3 illustrates the approach to determining optimal build direction/vector and Section 4 describes the optimal toolpath planning methodology with the consideration of resource consumption.

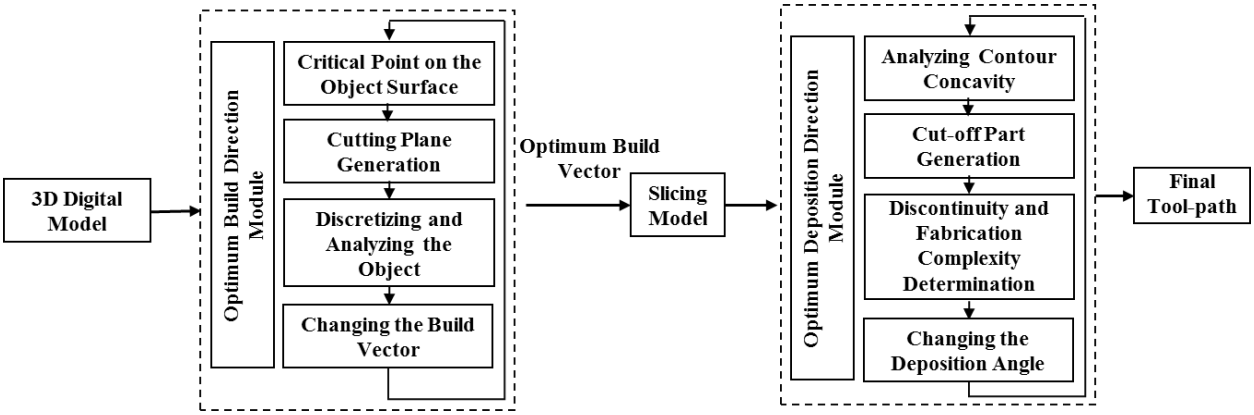

Figure 4. Workflow 1 of the proposed methodology.

Considering fabrication complexity resulting from the part geometric attributes, a concurrent process plan optimization framework is proposed and presented in Section 5. The workflow (2) of this methodology is shown in Figure 5.

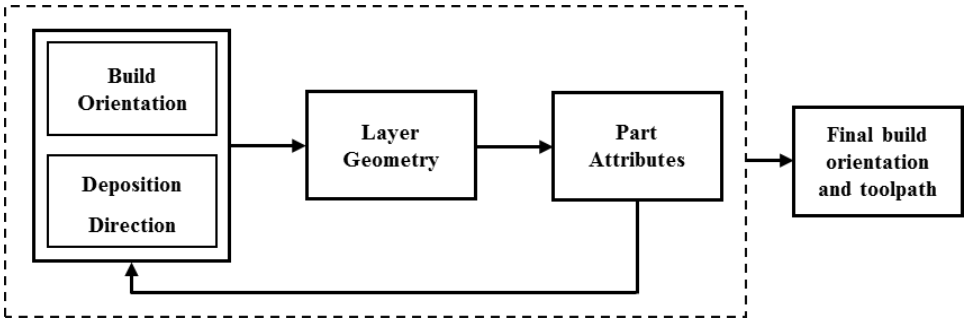

Figure 5. Workflow 2 of the proposed methodology.

Finally Section 6 concludes this work and presents some future directions of this research.

2. LITERATURE REVIEW

2.1. Additive Manufacturing

In additive manufacturing (AM) processes, commonly known as layer manufacturing or 3D printing, physical models are built layer-by-layer. The process plan starts with a digitized model and ends by stacking the individual printed layers along the build direction creating the 3D physical model. However, depending upon the AM technique and the process plan, the fabricated part may require post processing. Thus, the AM processes can be divided into three sequential technological steps: preprocessing (virtual), processing (actual printing), and post-processing as shown in Figure 6. Activities under each step directly contribute towards the fabricated part and optimizing one or more steps may improve the process capabilities. However, these activities are directional, i.e., they have a hierarchical relationship and the error that accumulates often time amplifies along the downstream activities.

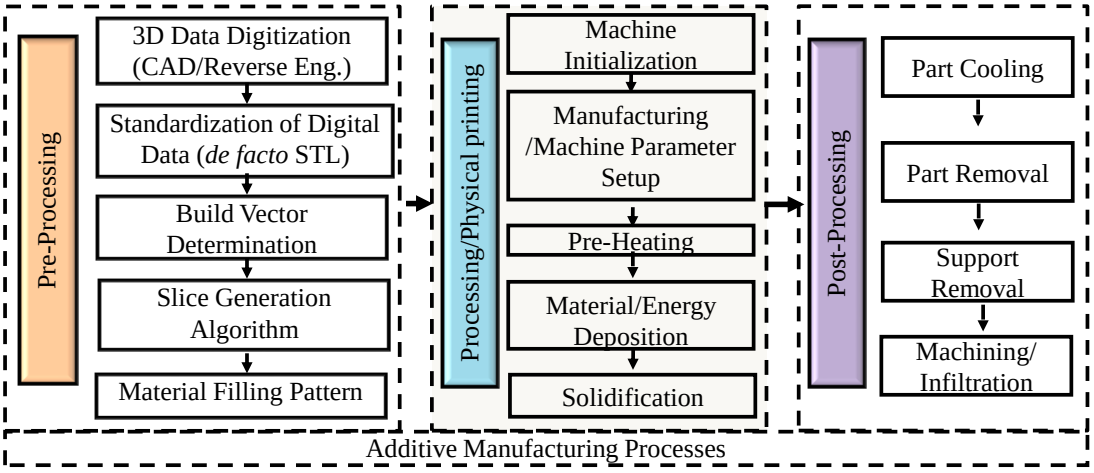

Figure 6. Hierarchical AM process plan.

The pre-planning/pre-processing stage is at the top of the AM hierarchy and can proactively alter the AM strategy into a guided desired outcome [30]. The pre-processing stage primarily uses computer aided design techniques to guide both the machine motion and material curing/deposition systems. This stage starts with design conceptualization and ends by

generating the AM process control instructions. The outcome of this stage is information, which is fully reversible based on the user requirement. Information from this stage is directed towards the processing stage where actual fabrication starts occurring and the process becomes irreversible.

2.2. Build Direction/Orientation

Build direction, which belongs to the virtual strategy, can be defined by the perpendicular vector on the imaginary plane for material deposition. Build direction attracted least attention from the AM research community and more or less considered as a user defined parameter [30]. When developing the process plan for AM, the build direction is a crucial factor to be considered. The most common assumption about build direction is that it affects the build time and the volume of support structure required during fabrication [31, 32]. Often, build direction is also associated with the number of layers of the part [33] to control the build time attribute. For the same part, any arbitrarily chosen build direction may result in a relatively larger build height, which would, in turn, definitely increase the number of layers and so the build time. Furthermore, surface quality of the part may also depend upon the build direction [1, 18]. Curved surfaces and the planer surfaces other than those which are either parallel or perpendicular to the selected build direction inherit poor surface quality due to the stepping effect of adding 2.5D layers one upon another in order to approximate the part surfaces [9, 34, 35].

Alexander *et al*. [1] determined build direction by maximizing the external surface accuracy through minimizing the average weighted cusp height. In bottom up AM technique, which requires support structure, the build direction is often confined with the planar (flat) surfaces of the object [33, 36, 37] as base. Xu *et al*. [31] proposed the selection of an optimum

building direction considering the differences of building inaccuracy, surface finish, and manufacturing time and cost for multiple additive manufacturing processes. An empirical knowledge based expert system tool developed by Frank [38] uses the expert questionnaire for decision matrix which helps establish the optimum or near optimal build direction.

The fabrication issue such as volumetric error [18] during deposition is also considered to find out an appropriate build direction. A multi-objective optimization method [39] is proposed to achieve good surface finish, accuracy and minimum build time. Byun and Lee [9] and Pham *et al.* [36] considered build time, surface quality, and cost of part to determine the optimum build direction from a set of pre-selected orientations. A proposition of a mathematical model to predict the layered process error considering the fabrication orientation is demonstrated by Lin et al. [40]. In order to improve the productivity, part quality, and economy during part fabrication, optimum orientation of part is determined by minimizing build time, staircase error, and material used [13] while maintaining the desired shell thickness. Tyagi *et al.* [17] modeled the optimal build orientation by considering the staircase effect and required build time. Both surface roughness and built time were used to determine the optimal part orientation for fused deposition modeling (FDM) system [5], selective laser sintering (SLS) and laminated object manufacturing (LOM) processes [3]. Thus, most of time build directions are selected to improve factors such as surface finish, build time and volume of support structure required, shrinkage, curling and part cost, but often time build direction is not the sole parameter that affect those factors. However, choice of the build direction can create multiple contours for free form shape object in the same layer which can increase the build time during fabrication.

2.3. Material Deposition/Filling Pattern

Once the build direction is defined, the model requires slicing. The 3D model is sliced by a set of parallel and intersecting planes perpendicular to the build direction. Closed 2D contours are generated by connecting the intersection points between the plane and the surface model. Material deposition path or tool-path is generated for individual slice with raster angle and hatch density to fill the internal space. The extruder or laser/light head need to be guided through the pre-defined contours or tool-path in order to create an internal meso-structure. Since each deposited layer is supported by its precedence layer, a 0°-90° raster angle pattern among successive layers is commonly used crisscrossing the meso-structure. However, other pre-determined layout patterns are tested for the structural integrity [29] and the attributes (i.e., pore size and geometry) [41] as well. Adaptive layout patterns [42] have recently been proposed by Khoda *et al.*to achieve the desired attributes i.e., porosity. Besides, a multi-directional parametric deposition orientation [43] is also proposed by considering the accessibility and porosity of the internal region. Too-path generation is the final step of the virtual strategy for affecting the attributes of the manufactured part. Physical strategies need to be deployed for better attributes as 2.5D layers are accumulated/cured and stacked successively to generate the 3D part. Depending upon the AM technique and the process plan, the fabricated part may require post processing i.e. cleaning extra material, heat treatment to diffuse adjacent layer etc.

2.4. AM Process Plan Solving procedure

Both build orientation and tool-path direction optimizations in AM processes are computationally intensive and multimodal problem. Rattanawong *et al.* [18] determined optimum build orientation using an exhaustive search method. Only one build orientation angle was varied at 15^{o} interval to minimize the volumetric error occurred in additively manufactured

parts. Ahsan *et al.* [15] generated the 3D build vector from two build orientation angles. Their two step process used a coarse resolution (10º) to identify the initial orientation candidate. Then a finer resolution (1º) is used to further explore the neighborhood and find the optimum build orientation considering build height, fabrication resource requirements, and surface quality. Part cylindricity error [44] was minimized to achieve geometric tolerances by incrementally rotating the part with 1º resolutions and thus finding the optimum build orientation. Ancaˇu and Caizar [3] determined pareto-optimal set of build orientations to optimize surface quality and build time by incrementally rotating the parts with 2º and 5º as well. Frank and Fade [45] developed an empirical knowledge based expert system using expert questionnaire for the decision matrix which helps selecting the optimum or near optimum build direction. Exhaustive search method was also used in an adaptive mixed tool-path generation algorithm [22, 46] to determine the best zigzag tool-path angle in order to optimize build time. However, these grid searching processes may require significant computational resources and may never reach optimal or near optimal solution. Alternatively, Tyagi *et al.* [17] used evolutionary stickers-based DNA algorithm to determine optimal build orientation. Their heuristic technique uses part attributes (i.e., volumetric error and build time) to determine the near optimal build orientation with finite number of iterations. The effectiveness of their objective function may be restricted to the complex geometry and concave layer contours.

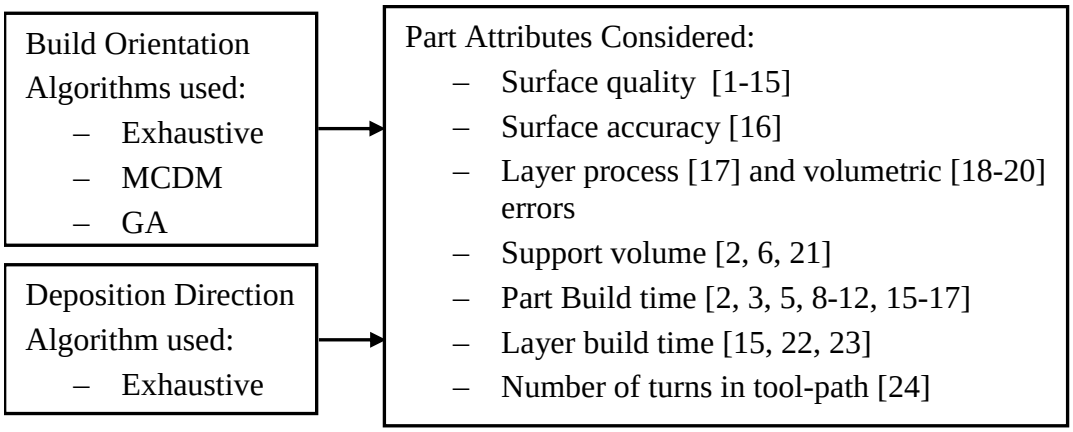

Figure 7. Different part attributes used to determine build orientation and tool-path direction.

2.5. Remarks

Figure 7 the parts attributes considered and solving procedures for AM virtual/pre-process planning problems reported in literature. It is clear from the above discussion that the part geometric attributes requiring more resources in terms of machine hour and energy have usually been ignored while determining process plans for additive manufacturing techniques.

3. BUILD ORIENTATION FOR AM PARTS

In this section a systematic framework is presented for build orientation determination to minimize the resource consumption during part fabrication.

3.1. Build Direction and Contour Plurality

Slicing an object that has concaved surface, for instance, the object shown in Figure 8, results in some slices that will contain more than one disjoint closed contour within each layer. In this thesis, this phenomenon is termed contour plurality. Contour plurality might also happen for objects with internal hollow features. The number of layers with contour plurality is fully dependent upon the build direction. For the same object, the overall contour plurality can be varied with different build directions as shown in Figure 8.

If the object shown in Figure 8 is sliced and then built layer by layer along the i^{th} build direction, several layers will have disjoint closed contours. While depositing material on these particular layers, it is not possible to achieve continuous deposition, thereby causing increased 'start-stops'. Besides, such disruption in deposition will impair the highly desired surface quality. If the machine is not responsive enough to start and stop depositing material precisely where it is needed, the exact shape of the object has to be sacrificed to some extent, causing volumetric error to increase. Overall, all these effects will increase the build time. Even though a machine might be highly responsive, it is necessary to avoid slice contour plurality to increase deposition continuity and in turn to achieve lower build time. On the other hand, there might be another build direction along which, if the same object is sliced and built layer by layer, there will be no, or a relatively less layers having disjoint closed contours. Thus, properly selected build direction for an object can significantly reduce the overall contour plurality throughout the layers and minimize the adverse effects of contour plurality. Conversely, choosing an arbitrary build

direction could result in most of the layers being contour plurality layers. Hence, the build vector along which the total volume of the object's regions having contour plurality layers is minimum can be considered favorable to resources.

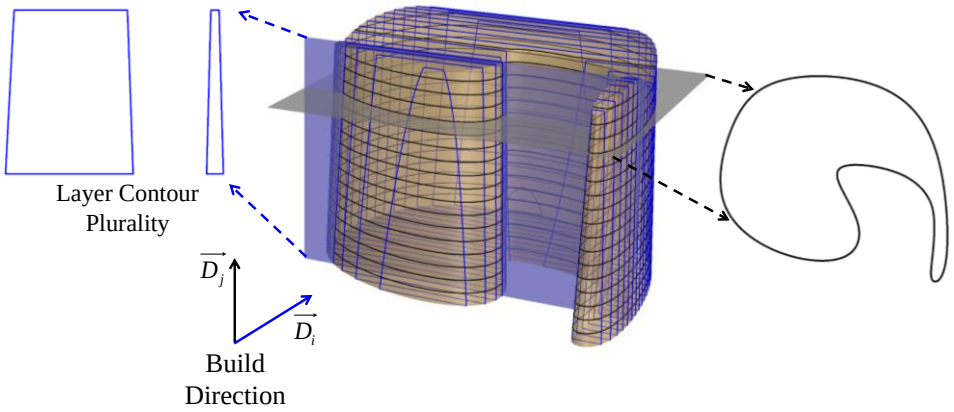

Figure 8. Build direction and contour plurality.

The build height and object features' sizes and shapes are other criteria which are also directly related to the resource requirement and may be affected by the build direction. Increased build height will increase the number of layers, thereby increasing the build time. The tiny or slender features of an object may result in contour plurality with tiny disjoint layer contours for a build direction. In this section, contour plurality, build height, object features' sizes and shapes, and surface quality are considered while finding out the proper build direction. An optimization algorithm is proposed to determine a build direction favorable to resources considering contour plurality and build height.

3.1.1. Quantification of Contour Plurality

To quantify the contour plurality in layers, first a build direction is generated through coordinate system transformation. Then the object volume is discretized considering the contour plurality along the build direction. This analysis is repeated for a number of build directions to quantify their effects on contour plurality as well as build height. In 3D Euclidian space $\Re^3$,

build direction can be represented as a 3D vector $\vec{D}_i = [x_i, y_i, z_i] \in \Re^3, \forall i = 0,...,n$. To determine a set of build vectors $\{\vec{D}_i\}_{i=1,...,n}$ the global coordinate system is rotated through ψ and φ angles around Z and Y axes, respectively [42], which can be represented by Eq. (1).

$$[x_i', y_i', z_i'] = [x_i \;\; y_i \;\; z_i] R_z(\psi) R_y(\varphi) \in \Re^3; \psi = [-\pi/2, \pi/2], \varphi = [0, 2\pi]; \forall i \tag{1}$$

where $R_z(\psi)$ and $R_y(\varphi)$ denote the rotation around Z and Y axis through ψ and φ angles, respectively. $[x_i', y_i', z_i']$ represents the transformed coordinate system, and the unit vector $\hat{\eta}_{z_i'}$ along Z_i' axis is considered as the corresponding build vector $\vec{D}_i$. Therefore, each build vector $\vec{D}_i$ corresponds to an angle pair (ψ, φ).

At any build direction $\vec{D}_i$, the object is discretized by a set of parallel planes $P_{k\,i}^i = \{aX_{i,k}' + bY_{i,k}' + cZ_{i,k}' = \text{constant}\}_{k=1,...,K}, \forall i$ that intersect the object surface. The parametric surface $S(u_i', v_i') \subset \Re^3$ of the object can be represented with parameter u_i' and v_i' where $u_i', v_i' \in [a_i, b_i]$. A set of finite number (L) of points $\mathbf{P}_i = \{p_l^i = (x_l^i, y_l^i, z_l^i)\}_{l=1,...,L}, \forall i$ associated with the corresponding parametric values $\mathbf{q}_i = \{(u_{i,l}', v_{i,l}')\}_{l=1,...,L}, \forall i$ is sampled on the surface $S(u_i', v_i')$. At all these sampled points, the surface's unit surface normal vectors $\vec{N}_l^i$ are determined which can be defined by Eq. (2).

$$\vec{N}_l^i = \frac{S_{u_i}(u_{i,l}', v_{i,l}') \times S_{v_i}(u_{i,l}', v_{i,l}')}{\left| S_{u_i}(u_{i,l}', v_{i,l}') \times S_{v_i}(u_{i,l}', v_{i,l}') \right|}, \quad l = 1,\text{K},L; \;\; \forall i \tag{2}$$

where $S_{u_i}(u_{i,l}', v_{i,l}') = \dfrac{\partial S(u_{i,l}', v_{i,l}')}{\partial u_{i,l}}$ and $S_{v_i}(u_{i,l}', v_{i,l}') = \dfrac{\partial S(u_{i,l}', v_{i,l}')}{\partial v_{i,l}}$. A point is defined as a critical point CP if $\vec{N}_l^i \cdot \hat{\eta}_{z_i'} = 1$ i.e., $S_{u_i}(u_{i,l}', v_{i,l}') = 0$, or $S_{v_i}(u_{i,l}', v_{i,l}') = 0$, which means that the surface's unit normal vectors at the critical points are parallel to the corresponding build vector. The critical

points are, therefore, the extreme points on the surface with respect to the build direction. Let a point set $\mathbf{CP}_i = \{cp_m^i\}_{m=1,\ldots,M} \subset \mathbf{P}_i$ contain only the critical points. A sorted critical point set $\mathbf{SCP}_i = \{scp_t^i = (x'_{scp_t}, y'_{scp_t}, z'_{scp_t})\}_{t=1,\ldots,T} \subset \mathbf{CP}_i$ is formed through sorting the critical points along the build direction $\vec{D}_i$ based on their perpendicular distance from the build plane and then discarding the redundant critical points. A rectilinear 3D bounding box [42] for the object is constructed along the transformed coordinate system using the vertex point set $\mathbf{V}_i = \{pt_1^i, pt_2^i, pt_3^i, \text{K}, pt_8^i\}$ defined by the combination of the minimum and maximum extents of the object's surface along the transformed X', Y', and Z' axes.

The plane on which the bottom bounding face of the bounding box lies, which is also perpendicular to the build direction $\vec{D}_i$, is considered the base plane or build plane of the object with respect to the coordinate system, as shown in Figure 9.

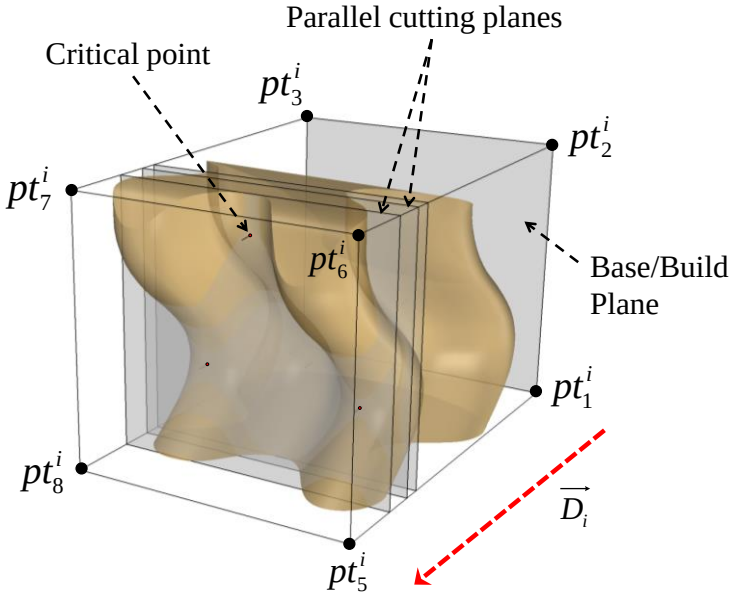

Figure 9. Bounding box generation and cutting planes through critical points.

In the i^{th} transformed coordinate system, if a point $p_t = (X_t', Y_t', Z_t')$ lies on the t^{th} cutting plane, a set of T number of cutting planes $\mathbf{CPL}_i = \{cpl_t^i\}_{t=1,\ldots,T}$ is generated through the sorted critical point set $\mathbf{SCP}_i$ using Eq. (3), which are parallel to the base plane.

$$\begin{bmatrix}\cos\psi.\cos\varphi & \sin\psi & -\cos\psi.\sin\varphi\end{bmatrix}\cdot\begin{bmatrix}X_t' - x_{scp_t}' \\ Y_t' - y_{scp_t}' \\ Z_t' - z_{scp_t}'\end{bmatrix} = 0; \quad t = 1,\ldots,T \tag{3}$$

After generating the cutting planes, the object volumes between the consecutive planes need to be evaluated for contour plurality. The object/part is split into $(T-1)$ strips with the generated parallel cutting planes forming the strip set $\mathbf{ST}_i = \{st_r^i\}_{r=1,\ldots,T-1}$. The total object volume generated between two consecutive parallel cutting planes cpl_t^i and cpl_{t+1}^i is termed as a part strip. If any strip contains more than one part split as shown in Figure 10, that part strip will comprise the layers with contour plurality along the corresponding build direction. So all the generated stripes are analyzed for contour plurality and a weight is determined for the corresponding build direction. The index i for build direction will be dropped to simplify the notations of some parameters and variables from now on.

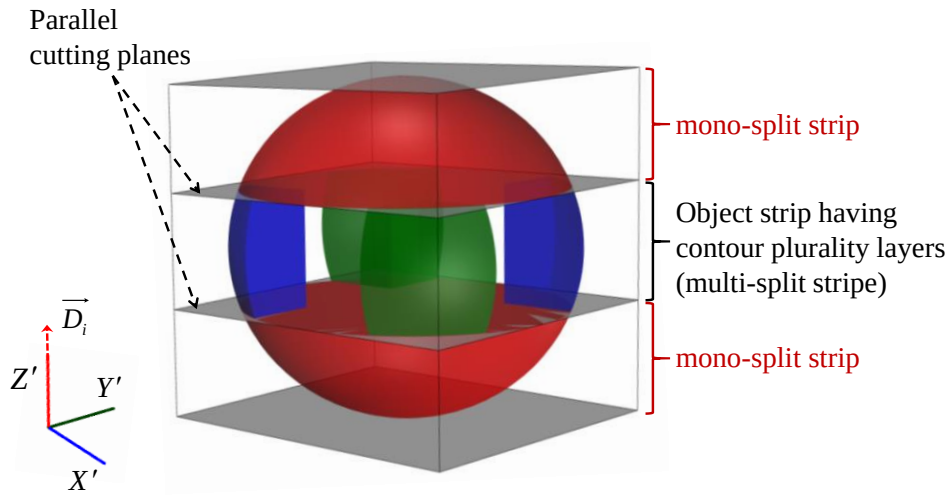

Figure 10. Cutting plane and contour plurality in strip.

The part strips generated by the parallel cutting planes can be classified as mono-split strip (red strips shown in Figure 10) and multi-split strip (middle strip in Figure 10) depending on the number of split part-volumes generated in the corresponding strip. Assume that r^{th} part strip contains a set $\{sp_f^r\}_{f=1,\ldots,F}$ of F number of split part-volumes. If $F=1$, the r^{th} part strip is a mono-split strip and if $F>1$, the r^{th} part strip is a multi-split strip. Multi-split strip may be generated if there is any concavity on the part surface or the part has one or more hollow features inside it. In a multi-split strip, the split part-volumes would yield multiple disjoint closed contours on the same layer. Thus, a build direction needs to be identified along which the total volume of the multi-split strips in regard to the total part volume would be minimum. Similarly, build height which usually changes with build direction directly affects the build time. A larger build height requires longer build time. When determining a desirable build direction taking contour plurality criterion into account, it is also necessary to ensure that the build direction does not lead to a considerably higher build height.

The build direction weight function corresponding to contour plurality for each part strip is, therefore, defined based on the number of split volumes existing in the strip and their volume values with respect to the total volume of the object. By summing up the volume of the split part-volumes, the total volume of each strip is calculated as

$$vol\_st_r^i = \left(\sum_{f=1}^{F} vol\_sp_f^r \right) \times w_r, \quad \forall r$$
$$\text{where,} \quad w_r = \begin{cases} 1, & \text{when } F>1 \\ 0, & \text{when } F=1 \end{cases} \tag{4}$$

Here, $vol\_st_r^i$ is the volume of r^{th} strip determined for i^{th} build direction, $vol\_sp_f^r$ is the volume of f^{th} split part-volume of r^{th} multi-split strip. Hence, the contour plurality volume fraction corresponding to i^{th} build direction can be evaluated as

$$VolF_i = \frac{\sum_{r=1}^{T-1} vol\_st_r^i}{vol\_part}, \qquad \forall i \tag{5}$$

where vol_part is the volume of the part and $VolF_i$ is the volume fraction of split part-volumes evaluated for i^{th} build direction. This volume fraction represents the total volume fraction of all the split part-volumes generated in multi-split strips of the object for the corresponding build direction, which is directly proportional to the total volume of the multi-split strips. The minimum possible value of the volume ratio is zero when there would be no multi-split strip i.e., no contour plurality in the layers throughout the whole part along a build direction.

3.1.2. Quantification of Shape Factor

Sometimes the part splits, i.e., split part-volumes, might be considerably tiny or thin which would lead to layers with fabrication complexity. For example, if the object is oriented and built along the direction $\vec{D}_i$ as shown in Figure 11, the thin feature of the object would result in thin layer contours which are susceptible to fabrication complexity. For some other build directions, there might be a lower number of layers or even no layers having tiny or thin contours. This fabrication issue is captured by analyzing the shape of the split part-volumes through using the bounding box technique to quantify the shape factor of the split part-volumes associated with the build direction. For each of the split part-volumes in a strip, a bounding box aligned with the build direction is generated and the shape factor is quantified, as discussed in Sections 3.1.2.1–3.1.2.3 for a single split part-volume and as shown in Figure 11. The same

procedure is applied for all the split part-volumes. Finally, the four elements are aggregated together to get the shape factor of the object for the corresponding build direction.

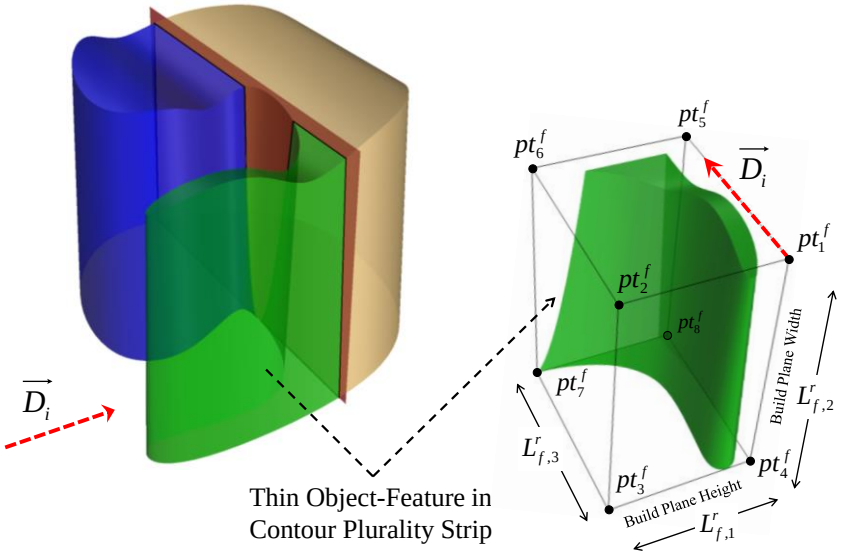

Figure 11. Thin object feature along a build direction and shape parameters.

3.1.2.1. Height/Width Factor

Height/Width (H/W) factor is used as one of the measures of fabrication complexity. A rectilinear bounding box aligned with the build direction is constructed for each split part-volume, as shown in Figure 11, to determine each split part-volume's H/W factor. The height component of the H/W factor is considered as the length of smaller side and the width component is considered as the length of larger side between two contiguous sides of the bounding box's top or bottom face. For the f^{th} split part-volume, if $L_{f,1}^r$ and $L_{f,2}^r$ are the lengths of the two sides of the bounding box's bottom or top face and $L_{f,3}^r$ is the length of the bounding box's other side which is parallel to the build direction, the H/W factor can be determined using Eq. (6).

$$H/W\_Factor_i = 1 - \frac{\sum_{r=1}^{T-1}\sum_{f=1}^{F}\left(\frac{H_f^r}{W_f^r}\right)\times vol\_sp_f^r}{vol\_part}, \quad \forall i$$

$$\text{where, } H_f^r = \min\left\{L_{f,1}^r, L_{f,2}^r\right\} \text{ and } W_f^r = \max\left\{L_{f,1}^r, L_{f,2}^r\right\}$$

$$H/W\_Factor_i = 1 - \frac{\sum_{r=1}^{T-1}\sum_{f=1}^{F}\left(\frac{H_f^r}{W_f^r}\right)\times vol\_sp_f^r}{vol\_part}, \quad \forall i \tag{6}$$

$$\text{where, } H_f^r = \min\left\{L_{f,1}^r, L_{f,2}^r\right\} \text{ and } W_f^r = \max\left\{L_{f,1}^r, L_{f,2}^r\right\}$$

Here, H_f^r is the height and W_f^r is the width of the f^{th} split part-volume in r^{th} strip along i^{th} build direction.

3.1.2.2. Build Plane Height and Build Plane Width Factors

For each split part-volume, the build plane height and width are assumed as the height and width of the corresponding split part-volume, as shown in Figure 11 and calculated in Section 3.1.2.1. For f^{th} split part-volume shown in Figure 11, H_f^r and W_f^r are the build plane height and width, respectively. To address the fabrication complexity, build plane height and build plane width factors are calculated by using the corresponding height and width and a given threshold value, assuming that fabrication complexity for the part splits will arise because of their tininess or slenderness when the build plane height, build plane width, or both values of the associated part splits are below the threshold value. The build plane height and width factors for i^{th} build direction, which are the volume weighted fraction deviations with respect to the threshold values, can be quantified by Eqs. (7) and (8), respectively.

$$BPHeight\_Factor_i = \frac{\sum_{r=1}^{T-1}\sum_{f=1}^{F} BPHeightR_f^r \times vol\_sp_f^r}{\sum_{r=1}^{T-1}\sum_{f=1}^{F} vol\_sp_f^r}, \quad \forall i \tag{7}$$

$$\text{where, } BPHeightR_f^r = \begin{cases} \dfrac{H_{thr}}{H_f^r}, & \text{when } H_f^r > H_{thr} \\ 1 - \dfrac{H_f^r}{H_{thr}}, & \text{when } H_f^r \le H_{thr} \end{cases}, \quad \forall\ f, r$$

$$BPWidth\_Factor_i = \frac{\sum_{r=1}^{T-1}\sum_{f=1}^{F} BPWidthR_f^r \times vol\_sp_f^r}{\sum_{r=1}^{T-1}\sum_{f=1}^{F} vol\_sp_f^r}, \quad \forall i \tag{8}$$

$$\text{where, } BPWidthR_f^r = \begin{cases} \dfrac{W_{thr}}{W_f^r}, & \text{when } W_f^r > W_{thr} \\ 1 - \dfrac{W_f^r}{W_{thr}}, & \text{when } W_f^r \le W_{thr} \end{cases}, \quad \forall\ f, r$$

Here, H_{thr} and W_{thr} are the given threshold values for build plane height and width, respectively, which are specified based on the machine capability and material type and composition. $BPHeightR_f^r$ and $BPWidthR_f^r$ are the fraction deviations of height and width, respectively, from the threshold values for the f^{th} split part-volume in r^{th} strip. $BPHeight\_Factor_i$ and $BPWidth\_Factor_i$ are the overall volume weighted build plane height and width factors, respectively, of the object for i^{th} build direction.

3.1.2.3. Fill Factor

In order to address how the material of a part split is distributed within its bounding box, fill factor takes into account the ratio of each part split's volume to the volume of their corresponding bounding box. Hence, this measure of shape factor captures how much the part splits fill their bounding box. If a part split fills its bounding box to a very low extent, fabrication complexity will again increase for that split. Eq. (9) symbolizes the fill factor.

$$Fill\_Factor_i = 1 - \frac{\sum_{r=1}^{T-1}\sum_{f=1}^{F}\left(\frac{vol\_sp_f^r}{vol\_BBox_f^r}\right)\times vol\_sp_f^r}{vol\_part}, \quad \forall i \tag{9}$$

where $vol\_BBox_f^r$ is the volume of the bounding box of f^{th} split part-volume in r^{th} strip aligned with i^{th} build direction.

3.1.2.4. Overall Shape Factor

The four normalized components of shape factor discussed above are aggregated together by summing up their weighted values as denoted by Eq. (10).

$$\begin{aligned} ShapeF_i = &\left(H/W\_Factor_i \times w_{HWF}\right) + \left(BPHeight\_Factor_i \times w_{HF}\right) \\ &+ \left(BPWidth\_Factor_i \times w_{WF}\right) + \left(Fill\_Factor_i \times w_{FF}\right) \end{aligned} \tag{10}$$

where $ShapeF_i$ is the aggregated shape factor of the object for i^{th} build direction and w_{HWF}, w_{HF}, w_{WF}, and w_{FF} are the associated weights for the four components of shape factor and their sum is unity. These weights reflect the relative importance of the associated factors and can be user defined. The Hypothetical Equivalents and Inequivalents Method (HEIM) [47] is utilized to determine the appropriate values of these weights analytically.

In Hypothetical Equivalents and Inequivalents Method, user gives the preferences, both equality and inequality, among the hypothetical alternatives. Here, the hypothetical alternatives are the hypothetical build directions. A set of constraints are formed using the preference which is shown by Eq. (11). Each constraint represents the preference between any two build directions in terms of their corresponding weighted sum of factor values. The weights are the decision variables and the objective is to make the sum of the weights one. Finally, the weights are generated by solving the minimization model.

$$
\begin{aligned}
&\text{Min} \quad [1-\sum_{\rho} w_{\rho}]^2 \\
&\text{s.t.} \\
&\sum_{\rho} F_{\rho}^{\upsilon} w_{\rho} - \sum_{\rho} F_{\rho}^{\tau} w_{\rho} \le -\delta; \quad \upsilon,\tau = 1,2,\text{K}\ ,\lambda \text{ and } \upsilon \ne \tau \\
&0 \le w_{\rho} \le 1; \quad \forall \rho
\end{aligned}
\tag{11}
$$

Here, ρ is the index for factors and w_{ρ} is the weight assigned to ρ^{th} factor. F_{ρ}^{υ} and F_{ρ}^{τ} are the values of the ρ^{th} factor obtained for υ^{th} and τ^{th} hypothetical build directions, respectively. The constraints are formulated given that υ^{th} hypothetical build direction is preferred to τ^{th} hypothetical build direction. δ is a small positive number which is used to ensure the inequality between two alternative hypothetical build directions. The optimization problem given by Eq. (11) is solved by using the constrained nonlinear minimization routine provided in MATLAB package.

3.1.3. Quantification of Surface Quality and Build Height

Surface quality of additively manufactured objects largely depends on the build direction which yields the object orientation during fabrication. The staircase effect between the consecutive layers impairs the surface quality of AM objects. There will be almost no staircase effect for an object oriented along a build direction when the build direction will be parallel or perpendicular to the surface of the object. In order to quantify the surface quality with respect to the build direction, the angles $\{\theta_g^i\}_{g=1,\ldots,G}$ between the build direction and the facet normal $\{\vec{F}_g\}_{g=1,\ldots,G}$ of the triangulated mesh model of the object having total G number of triangular facets are identified, as shown in Figure 12. It is assumed that the staircase effect, due to a facet, exists over the whole area of the triangular facet. Therefore, when the facet normals are either parallel $(\theta_g^i = 0°)$ or perpendicular $(\theta_g^i = 90°)$ to the build direction, the staircase effect will be

minimum giving good surface quality. Staircase effect will be maximum giving poor surface quality when the facet normal is aligned at 45° with the build direction. The surface quality index for each facet, e.g., g^{th} facet shown in Figure 12, can be determined using Eq. (12).

$$SQIndex_g^i = \begin{cases} 0, & \text{when } \theta_g^i = 0°,\ 90°,\ \text{or } 180° \\ \left|\tan\theta_g^i\right|, & \text{when } 0° < \theta_g^i \le 45°,\ \text{or } 135° < \theta_g^i < 180°, \\ \dfrac{1}{\left|\tan\theta_g^i\right|}, & \text{when } 45° < \theta_g^i < 90°,\ \text{or } 90° < \theta_g^i \le 135° \end{cases} \quad \forall g \tag{12}$$

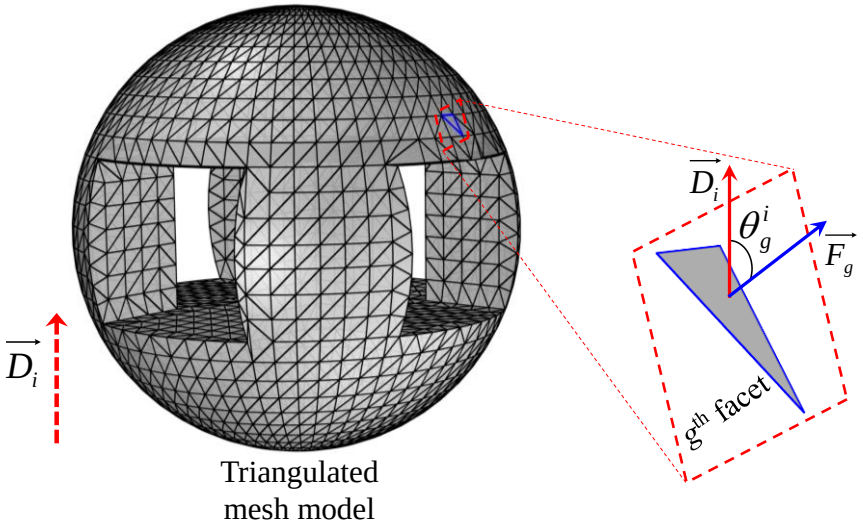

Figure 12. Facet normal and surface roughness.

The surface quality factor of the entire object for i^{th} build direction is quantified by averaging the facet surface quality indices $\{SQIndex_g^i\}_{g=1,\ldots,G}$ with the corresponding facet areas as

$$SQF_i = \frac{\sum_{g=1}^{G} SQIndex_g^i \times FA_g}{\sum_{g=1}^{G} FA_g}, \quad \forall i \tag{13}$$

where SQF_i denotes the surface quality factor of the object determined for i^{th} build direction and FA_g is the area of g^{th} facet of the object surface. Build height which usually changes with build direction directly affects the build time. The larger the build height, the longer the build time is. So while determining a good build direction considering the other phenomena discussed above, it is also necessary to ensure that the build direction does not lead to a considerably higher build height. For i^{th} build direction, the build height (BH) of the part is determined as the height of part's bounding box along that build direction and then normalized to get the build height factor (BHF).

3.1.4. Determination of Optimal Build Direction

The objective function to determine an optimal build direction, which will be the weighted sum of normalized contour plurality volume fraction, shape factor, surface quality factor, and build height, is expressed as

$$TotalWeightBD_i = (VolF_i \times w_{CP}) + (ShapeF_i \times w_{SF}) + (SQF_i \times w_{SQ}) + (BHF_i \times w_{BH}), \forall i \quad (14)$$

where $TotalWeightBD_i$ is the overall weight determined for the build direction $\vec{D}_i$. w_{CP}, w_{SF}, w_{SQ}, and w_{BH} are the weights for contour plurality volume fraction, shape factor, surface quality factor, and normalized build height, respectively. The optimal values of these weights are determined using HEIM [47] discussed in Section 3.1.2.4. Finally, the optimum build direction can be determined solving the following minimization problem.

$$\begin{aligned} &\text{Min} \ \{TotalWeight\_BD_i\}_{i=1,\text{K},n} \\ &\text{s.t.} \\ &\overrightarrow{D_i} := \hat{\eta}_{z_i'} \\ &\psi = [-\pi/2, \pi/2] \\ &\varphi = [0, 2\pi] \end{aligned} \quad (15)$$

where $\{TotalWeightBD_i\}_{i=1,\ldots,n}$ is a set of objective function values, which can also be termed as a set of overall weights of the build directions. The individual elements of this set can be calculated with Eqs. (4)–(10), (12), and (13).

Each build direction $\vec{D}_i$ and hence the transformed coordinate system $[x_i', y_i', z_i']$ for Eq. (15) can be constructed by rotating the standard coordinate system around Z and Y axes with angle $\psi \in [-\pi/2, \pi/2]$ and $\varphi \in [0, 2\pi]$, respectively. The following greedy heuristic is applied to determine the optimum build direction using Eq. (15). First, a candidate set of finite number of build directions $\{(\psi, \varphi)\}$ is formed at a uniform interval γ on both ψ and φ. From this candidate set, the build directions with the lowest objective function value are chosen. Their neighborhoods are then explored with higher resolution λ, where $\lambda << \gamma$. The transformed Z axis vector corresponding to the angle pair (ψ^*, φ^*) that yields the minimum objective function value is selected as the optimal build direction.

3.2. Implementation

The proposed methodology is implemented on two example objects as shown in Figure 13 and Figure 15 with a Core i7 @ 3.4 GHz CPU with 4 GB RAM using Visual Basic scripting language. Total time needed to implement the methodology on example 1 and example 2 are approximately 15 and 9 seconds per iteration, respectively. However, the required time can be reduced significantly by parallel processing or increasing the computational power.

Example 1 containing both contour plurality and layer contour concavity, which is shown in Figure 13(a), is used to demonstrate the proposed methodology. The object has a volume of 56130 cubic mm with a number of 16806 triangular facets. The resolutions: $\gamma = 10°$ and $\lambda = 1°$, and weight values: $w_{CP} = 0.5$, $w_{BH} = 0.2$, $w_{SF} = 0.1$, $w_{SQ} = 0.2$, $w_{HWF} = 0.15$, $w_{HF} = 0.38$,

$w_{WF} = 0.28$, and $w_{FF} = 0.19$ are used for Eq. (15) during implementation. The optimum build direction generated from the proposed algorithm is $\psi^* = 11°, \varphi^* = 304°$ as shown in Figure 13(b). The objective function values for different build directions are mapped in 3D space and represented in Figure 14.

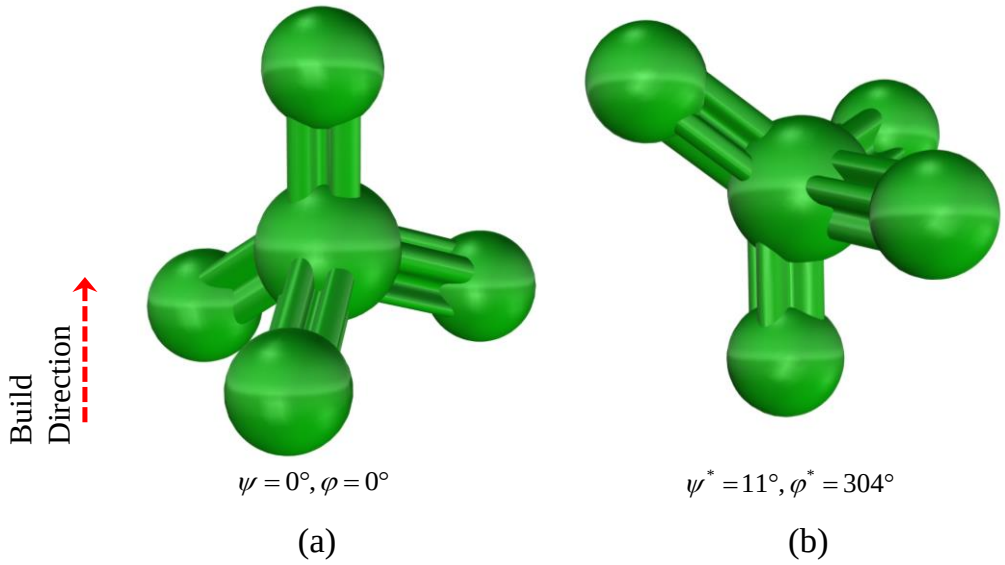

Figure 13. (a) Example 1 with reference ($\psi^* = 0°, \varphi^* = 0°$) and (b) Example 1 oriented along the optimal build direction ($\psi^* = 11°, \varphi^* = 304°$).

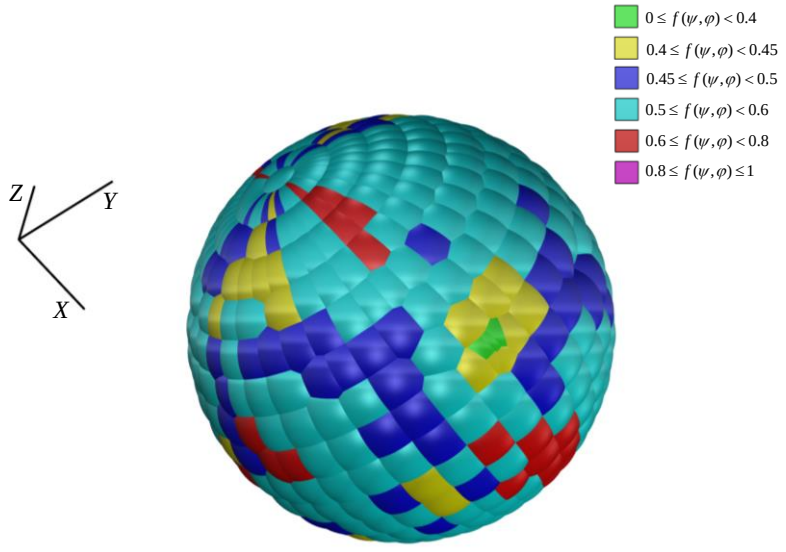

Figure 14. Build direction vectors and objective function values for first example are mapped in 3D space.

Table 1 summarizes the results for the optimal build angle pair and some other arbitrary build angle pairs. The result shows the independent nature of each factor as their values vary based on the build direction. The methodology discussed in Section 3.1 yields the minimum objective function value at (11°, 304°).

Table 1. Results for different build directions of Example 1.

ψ	φ	Plurality Volume Factor	Build Height Factor	Shape Factor	Surface Quality Factor	Total Weight
–90	0	0.378	0.887	0.849	0.453	0.542
–80	10	0.291	0.949	0.894	0.463	0.517
–80	20	0.214	0.969	0.914	0.458	0.484
–70	15	0.185	0.959	0.908	0.459	0.467
–60	200	0.259	0.980	0.891	0.461	0.507
–60	300	0.863	0.871	0.799	0.483	0.782
–40	30	0.206	0.992	0.912	0.461	0.485
–10	90	0.075	0.896	0.939	0.473	0.405
0	0	0.378	0.887	0.849	0.453	0.542
10	300	0.086	0.887	0.935	0.454	0.405
11	**304**	**0.036**	**0.910**	**0.941**	**0.454**	**0.385**
30	20	0.434	0.932	0.851	0.468	0.582
40	150	0.337	0.951	0.873	0.449	0.536
60	40	0.158	0.971	0.922	0.456	0.457
80	300	0.523	0.856	0.879	0.480	0.617

A second example shown in Figure 15(a), is used to again demonstrate the effectiveness of the proposed methodology. This example 2 object has a volume of 15166 cubic mm with a number of 3372 triangular facets. The following weight values are used to apply the methodology: $w_{CP} = 0.40, w_{BH} = 0.21, w_{SF} = 0.19,$ and $w_{SQ} = 0.19$. Resolutions and other weight

values used for Eq. (15) and (22) are same as that of example 1. The optimum build direction generated from the algorithm is $\psi^* = 0°, \varphi^* = 356°$ as shown in Figure 15 (b).

The optimum build vector ($\psi^* = 0°,\ \varphi^* = 356°$) yields the minimum objective function value. If the part is built along this direction, there would be only 0.1% contour plurality volume of the total volume of the object. Compared to an arbitrary direction (–20°, 80°), contour plurality, build height, and fabrication complexity (shape factor) are decreased by 91.2%, 30%, and 65%, respectively. The total build time for the optimal build direction, $\psi^* = 0°, \varphi^* = 356°$, is also reduced by 7.8% compared to an arbitrarily selected build direction $(\psi = -20°, \varphi = 80°)$. The objective function values for this example at different build directions are mapped in 3D space and represented in Figure 16. The objective function value shown in the 3D map follows a pattern along one axis due to the axisymmetric attributes of the object.

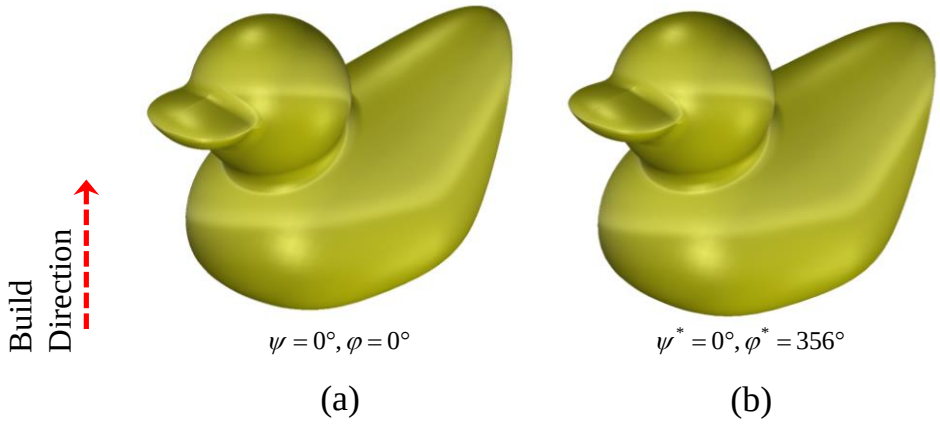

Figure 15. (a) Example 2 with reference ($\psi^* = 0°, \varphi^* = 0°$) and (b) Example 2 Oriented along the optimal build direction ($\psi^* = 0°, \varphi^* = 356°$).

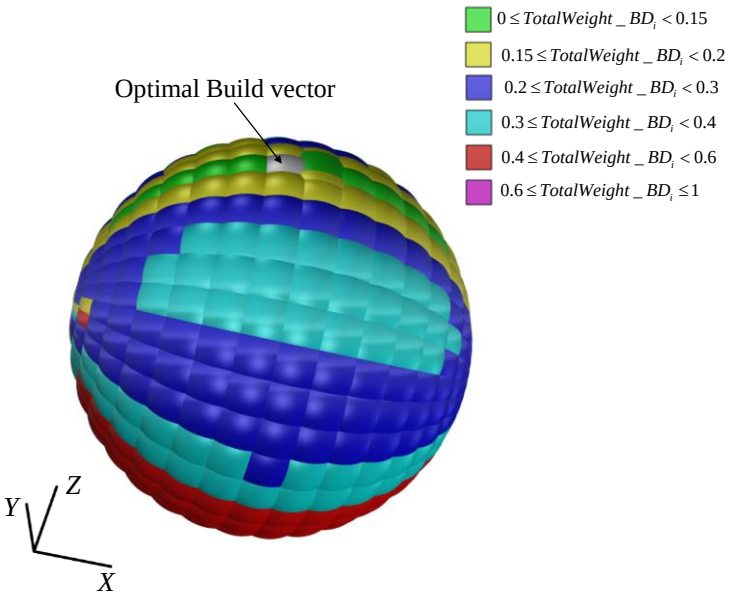

Figure 16. Build direction vectors and objective function values for second example are mapped in 3D space.

3.3. Remarks

An AM process planning approach emphasizing on the build direction has been developed in this Section which allows the minimum usage of resources. The outlined methodology proposes an optimal build direction considering the lower contour plurality, build height, fabrication complexity, and better surface quality. The optimal build direction minimizes the total build time by reducing the contour plurality as well as improves the surface quality by reducing the stair-case effect. The next step is to orient and slice the part along the optimal build direction and to determine optimal toolpath directions for each layer which is discussed in Section 4.

4. TOOLPATH PLAN FOR AM PARTS

The object is sliced along the resource favorable build direction (described in Section 0) by a set of intersecting planes parallel to each other. The non-self-intersecting, closed, and planar layer contours which will represent the object are generated by connecting the intersection points between each intersecting plane and the object surface. The distance between the consecutive intersecting planes is kept constant which is the diameter of the filament to be deposited. This uniform slicing results in a set of contours, $\mathbf{C} = \{C_k\}_{k=1,2.....K}$ for depositing material layer-by-layer. The following analysis has been done for a specific contour. As all the contours are planar closed curves, they only intersect to their start and end points. These contours can be parametrically represented by Eq. (16).

$$\begin{aligned} &C_k(u_k) = (x(u_k), y(u_k)), \text{ where } k = 1,2,\text{K},K \\ &u_k \in [a_k, b_k] \\ &C_k(a_k) = C_k(b_k) \end{aligned} \tag{16}$$

Where $C_k(u_k)$ represents the parametric curve of k^{th} contour with respect to the parameter u_k ranging between $[a_k, b_k]$. The presence of contour plurality in the object will result in a set of contour on the same layer and that can be represented as $\mathbf{L} = \{\mathbf{L}_y\}_{y=1,2,\text{K},Y}$ and $\mathbf{L}_\mathbf{y} = \{C_k\}$ where, $k > 1$ and $\mathbf{L}$ stands for a set of layer contours.

4.1. Tool Path Angle and Layer Contour Concavity

Concavity is the property of curving a graph of the function upward or downward. In 3D free-form shaped object, the layer contour may contain curving upward (minima) and downward (maxima). In between of two adjacent minima or maxima on a layer contour curve, there will be a maxima or minima, respectively, as shown in Figure 17. During material deposition across these adjacent maxima or minima, the print head has to stop, pass through air, and then start

material deposition again as shown in Figure 17(a). The deposition direction across the adjacent minima or maxima, therefore, introduces deposition discontinuity as well as two cut-off parts in layers.

Because of deposition discontinuity, the print head frequently starts and stops during deposition as shown in Figure 17(a), and causes over-deposition. This costs resources such as time and material for over deposition which is not good for the surface integrity and dimensional accuracy of the finished part [3]. Therefore, a suitable material deposition direction for each layer needs to be determined in order to minimize the resource requirements for the concave layer contours.

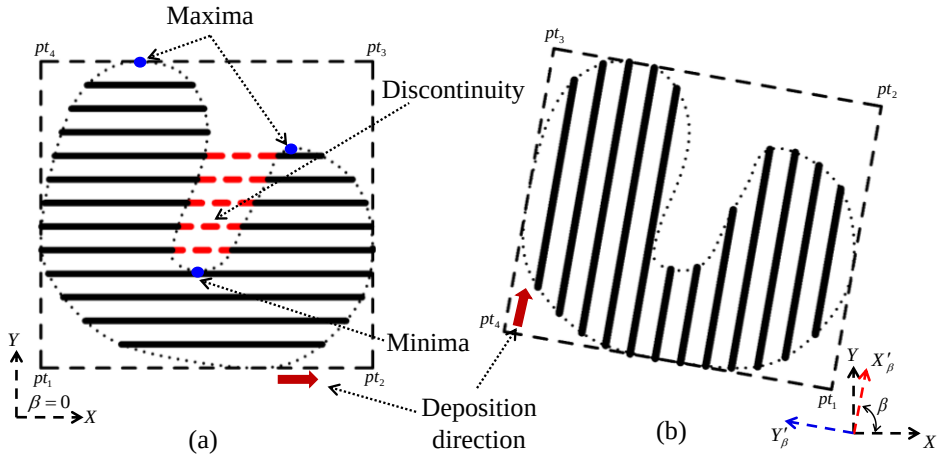

Figure 17. Layer contour concavity. (a) discontinuity and (b) no discontinuity along X'_β axis.

4.1.1. Quantification of Slice Concavity

To analyze each layer contour, a 2D rectilinear bounding box of each 2D layer contour is constructed as shown in Figure 17. To get a set of deposition directions, the coordinate system is rotated around Z axis through β angle where $\beta \in [0, \pi]$. Each time the transformed X'_β axis vector is considered as the deposition direction. In a transformed coordinate system, a set of tangent vectors, $\mathbf{T} = \{t_j\}_{j=0,1,\ldots,N}$ is considered on the layer contour at N number of equidistant

points and the transformed X'_β axis vector is regarded as the base vector $(\vec{B})$. The points on the contour curve at which the first derivatives of the curve (tangent vectors) with respect to X'_β axis are zero, are the stationary or extreme points of the curve.

The set of extreme points can be represented as $\mathbf{E} = \{e_n\}_{n=0,\ldots,N'}$. If more than two extreme points exist on a contour, there will be discontinuity for a number of deposition directions and the print head will pass through the air as shown in the Figure 17(a). The straight lines passing through the extreme points $(\mathbf{E})$ and parallel to X'_β (the base vector) are defined as cutting lines which constitute the cutting line set $\mathbf{CL} = \{l_c\}_{c=0,\mathrm{K},m}$ where $m \le N'$. The area of the contour curve between two adjacent cutting lines (l_c, l_{c+1}) is denoted as a strip. The generated strips are classified as continued and discontinued strips. The strips $\mathbf{S_T} = \{S_t\}_{t=0,\mathrm{K},(n-1)}$ which contain the start-stop event or discontinuity or the cut-off contour parts are considered as discontinued strip as shown in Figure 18. The continued strip containing no start-stop event or cut-off part is more expected in layer manufacturing.

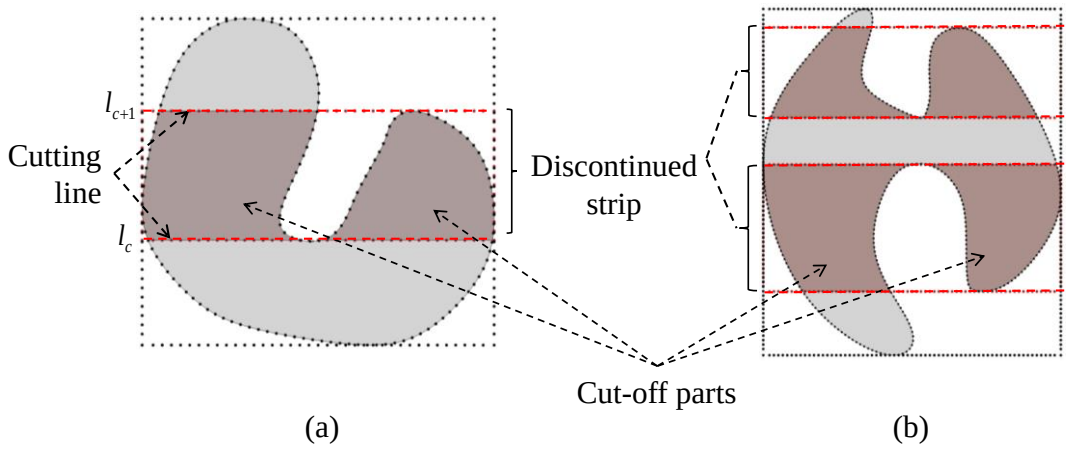

Figure 18. Discontinued strips in contour. (a) single strip and (b) multiple strips.

For the set of cut-off parts $\mathbf{P} = \{p_x\}_{x=0,\mathrm{K},X}$ of a contour curve obtained for a deposition direction, the total area of the cut-off parts and discontinuous area factor can be calculated by Eq. (17).

$$DAF^k = \frac{\sum_{x=o}^{X} C_x}{Area^k}, \qquad \forall k \tag{17}$$

where C_x is the area of x^{th} cut-off part, $Area^k$ is the total area, and DAF^k is the discontinuous area factor of the k^{th} contour. The larger the value of discontinuous area factor, the more resources will be consumed.

4.1.2. Quantification of Contour Shape Factor

Once the contour contains cut-off parts, each part is analyzed for fabrication complexity. Shape of the contour plays a significant role to determine fabrication complexity. For example, contour with tiny feature or segment is difficult to produce. Even though, build direction methodology minimizes such slender feature generation, many times it would not be possible to eliminate this completely. Thus, some layer contour may still end up with tiny features after slicing and proper deposition direction may minimize their adverse effect. To quantify the layer-wise fabrication complexity for tiny features, the shape factor consisting of aspect ratio and fill factor of each cut-off part is calculated and finally, the overall contour shape factor is determined for a deposition direction.

4.1.2.1. Aspect Ratio

An aspect ratio of a geometric shape normally reflects the ratio between its sizes in different dimensions. If each cut-off part of a layer contour is inscribed by a rectilinear 2D bounding box, the ratio of shorter dimension to larger dimension of this bounding box is

considered as aspect ratio of this part as shown in Figure 19 and the area weighted aspect ratio for the entire layer contour can be determined by Eq. (18).

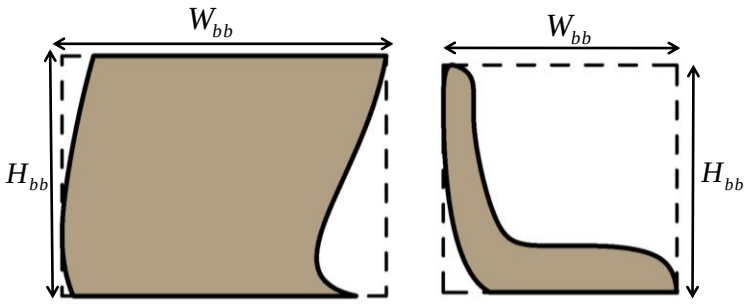

(a) (b)

Figure 19. Aspect ratio of Cut-off parts in contour curve. (a) low and (b) high fill factor.

$$AR^k = 1 - \frac{\sum_{x=1}^{X} AR_x \times C_x}{Area^k}, \quad \forall x \tag{18}$$

$$\text{where, } AR_x = \begin{cases} \frac{H_{bb}^x}{W_{bb}^x}, & when\ W_{bb}^x > H_{bb}^x \\ \frac{W_{bb}^x}{H_{bb}^x}, & when\ H_{bb}^x > W_{bb}^x \end{cases}, \quad \forall x$$

Here, AR_x is aspect ratio of x^{th} cut-off part, AR^k is the total aspect ratio for k^{th} contour, and W_{bb}^x and H_{bb}^x are the width and height of the bounding box, respectively, of x^{th} cut-off part.

4.1.2.2. Contour Fill Factor

Often time the aspect ratio may not reflect the actual shape of the cut-off part as shown in the Figure 19(b). Another factor namely contour fill factor is incorporated to have the better sense of shape. The ratio between the total area of cut-off parts and the area of its bounding box is considered as contour fill factor. The fill factor for a contour can be determined as

$$CFF^k = 1 - \frac{\sum_{x=1}^{X} \frac{C_x}{BBArea_x}}{Area^k}, \quad \forall k \tag{19}$$

where $BBArea_x$ is the area of the bounding box of x^{th} cut-off part, and CFF^k is the fill factor for k^{th} contour. The less value of contour fill factor reflects ease of deposition on the corresponding contour.

Finally, the total contour shape factor is considered as the weighted sum of aspect ratio and contour fill factor and represented by Eq. (20).

$$CSF_k = \left(AR^k \times w_{AR}\right) + \left(CFF^k \times w_{CFF}\right), \qquad \forall k \tag{20}$$

Where CSF_k is the contour shape factor for k^{th} contour, w_{AR} is the weight for aspect ratio, w_{CFF} is the weight for area factor. The optimal values of these weights are determined using the same HEIM method [47] discussed in Section 3.1.2.4.

4.1.3. Optimal Material Deposition Direction

To quantify the deposition direction, Eq. (1) in section 2.1 is used for one axis rotation and the coordinate system is rotated by β angle around the *Z*-axis. One sample example of two deposition directions along with corresponding area of cut-off parts is shown in the Figure 20.

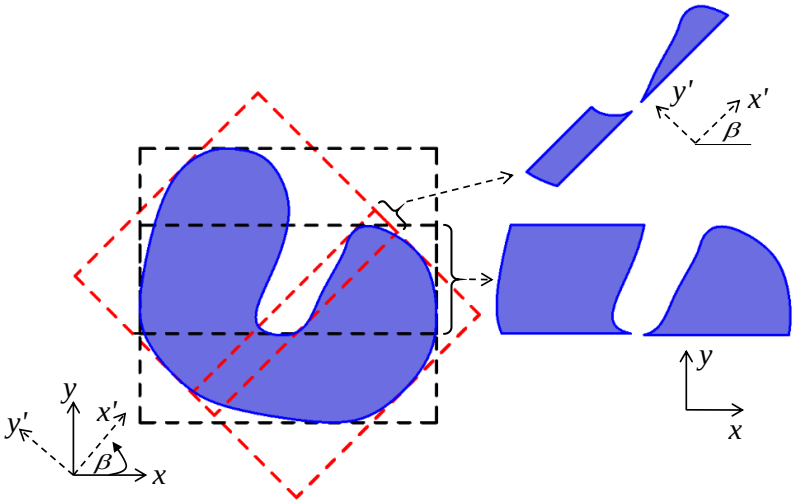

Figure 20. Cut-off parts of the same layer contour for two different deposition directions.

The ultimate weight for a deposition direction given by Eq. (21) is determined as the weighted sum of the discontinuous area factor and the contour shape factor.

$$weight\_DD_k^{\beta} = (DAF_k \times w_{DAF}) + (CSF_k \times w_{CSF}), \qquad \forall k \tag{21}$$

where $weight\_DD_k^{\beta}$ is the ultimate weight of β deposition angle for k^{th} contour, w_{DAF} is the weight for discontinuous area factor, w_{CSF} is the weight for contour shape factor. The HEIM technique [47] discussed in Section 3.1.2.4 is also used here to determine the optimal values of these weights. The model for finding optimal material deposition direction can be represented by Eq. (22).

$$\begin{aligned} &\text{Min} \ \{weight\_DD_k^{\beta}\} \\ &\text{s.t.} \\ &\beta \in [0, \pi] \\ &\beta_y \notin (\beta_{y-1} - \phi, \beta_{y-1} + \phi), \qquad \forall y \\ &\phi \geq 0 \end{aligned} \tag{22}$$

The optimal material deposition direction i.e., tool path orientation angle can be determined by solving the optimization problem presented by Eq. (22) using the same method explained in section 2.4. While determining the optimal tool path orientation angles for consecutive layers, a tabooed range of angle defined by $\pm\phi$ must be imposed for the consecutive layers to ensure the structural continuity and integrity of layers. Hence, the material deposition angle depends on the angle of the supporting layer. If the deposition angle of y^{th} layer is β^*, the acceptable deposition angle of $(y+1)^{\text{th}}$ layer cannot lie within the range $\beta^* \pm \phi$.

Once the optimal build direction and deposition direction are obtained, the total build time is measured to validate the proposed methodology. The total fabrication/build time of an object can be classified into two components: deposition time and air/non-deposition time [48] as shown in Eq. (23). The total air time will be the summation of air time for contour plurality and

contour concavity. During the calculation of deposition time, if the deposition length is greater than a threshold value T_h for any segment, three stages of motion namely acceleration stage, constant speed stage, and deceleration stage are considered [49]. If the filament size is smaller than the threshold value T_h, only the acceleration and deceleration stages are considered.

$$BuildTime_{(\psi,\varphi)} = \sum_{y=1}^{Y} \left(LBT_y^{\beta} + LAT_y^{\beta} \right) \tag{23}$$

where $BuildTime_{(\psi,\varphi)}$ is the total build time of an object oriented along (ψ,φ) build direction. LBT_y^{β} and LAT_y^{β} are the build and air time, respectively, of y^{th} layer for β deposition angle.

4.2. Implementation

After getting the optimal build directions for the two example objects used for the implementation of the methodology given in Section 3.2, both objects are oriented as shown in Figure 13(b) and Figure 15(b). Then the objects are sliced along that direction using uniform slice thickness given in Table 2. The resulting layer contours are analyzed individually and consecutively following the methodology discussed in Section 4.1 in order to determine their optimal material deposition directions. Thus, layer wise deposition directions for the entire 3D object are generated to address the resource consumption. During the implementation, the resolution for Eq. (22) is used as $\gamma = 5°, \phi = 45°$ and the weights used are $w_{AR} = 0.5, w_{CFF} = 0.5, w_{DAF} = 0.7, w_{CSF} = 0.3$. Five layer contours of Example1 object are taken at different arbitrary height locations along $\psi^* = 11°, \varphi^* = 304°$ as shown in Figure 21 and the fabrication time is measured using Eq. (23). The fabrication parameters considered to measure the time is shown in Table 2 which are adopted from Dimension® bst 1200es FDM machine from Stratasys.

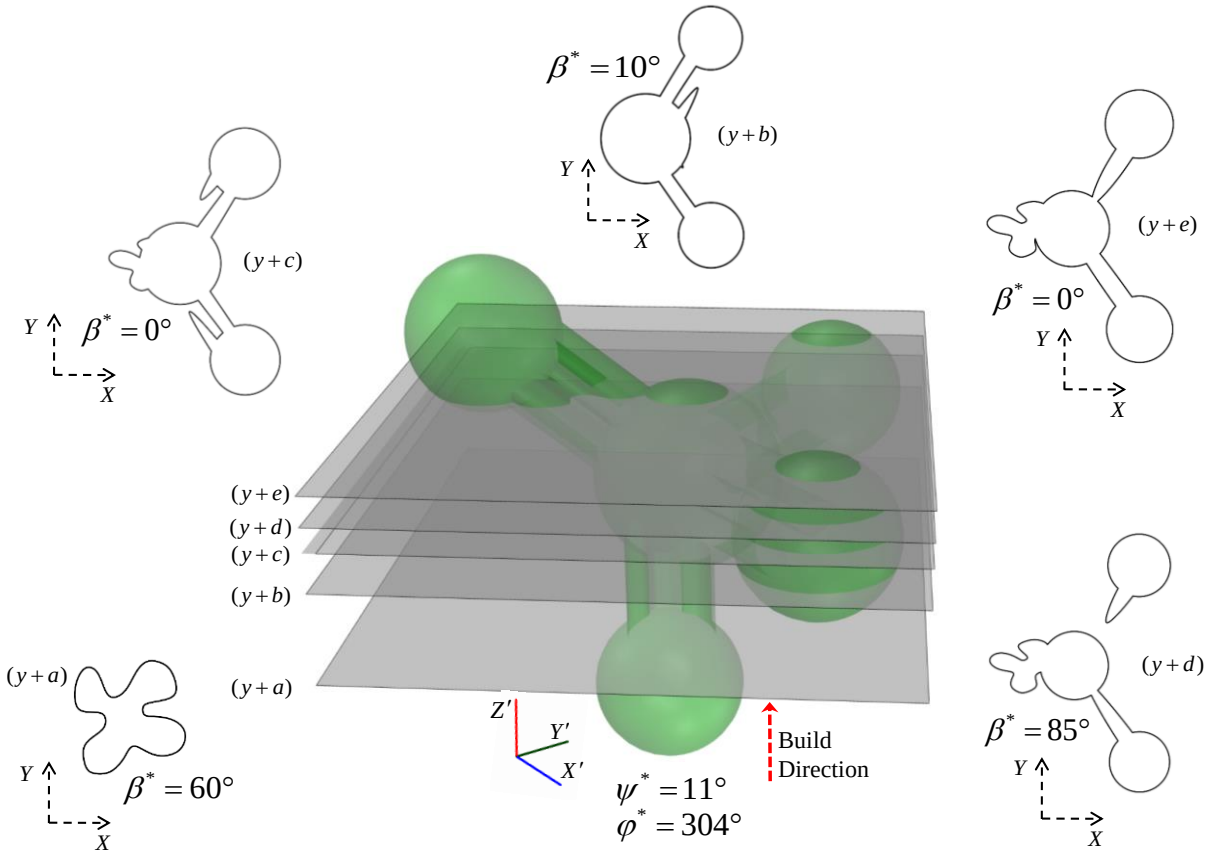

Figure 21. Contours of Example 1 object at different layers with best deposition directions.

Table 2. Fabrication parameters [Dimension® bst 1200es from Stratasys].

Slice thickness	0.254 mm
Raster Width	0.5 mm
Travel Speed	7800 mm/min
In-Fill Speed	3048 mm/min

To analyze the result further, contour cut-off parts (discontinuous area), deposition travel lengths of tool, non-deposition travel lengths of tool, and total layer deposition times are measured for the whole object (example 1) and shown in Table 3. All of these measured metrics show minimum values for the optimum directions as shown in Table 3. Two arbitrarily selected layers $(y+a)^{\text{th}}$ and $(y+c)^{\text{th}}$ are analyzed and the result are shown in Figure 22–23.

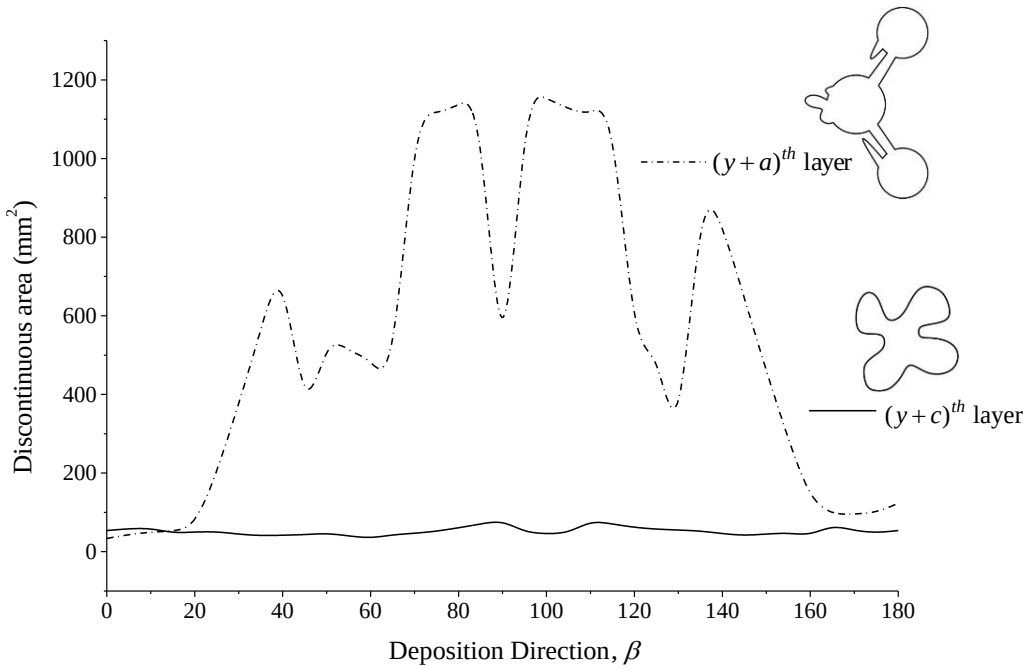

Figure 22. Discontinuous contour areas of two layers for different deposition directions of Example 1.

Table 3. Process plan results for different build directions

ψ	φ	Deposition length (mm)	Non-deposition length (mm)	Total length (mm)	Deposition time (min)	Non-deposition time (min)	Total time (min)	% Improve-ment of length	% Improve-ment of time
1	304	224385	6844	231229	281	25	306	17.87%	20.73%
0	0	225836	30565	256401	282	64	354	8.93%	8.29%
30	150	234994	38680	273674	298	76	373	2.79%	3.37%
10	60	235262	46269	281531	294	92	386	0.00%	0.00%
73	253	232514	40907	273421	291	84	375	2.88%	2.85%
–25	75	234856	35113	269969	293	72	365	4.11%	5.44%
–53	175	232314	31856	264170	290	67	357	6.17%	7.51%
–20	30	237539	20882	258421	297	39	336	8.21%	12.95%
–40	100	232827	35340	268167	291	72	363	4.75%	5.96%
–70	20	237007	37380	274387	296	72	368	2.54%	4.66%

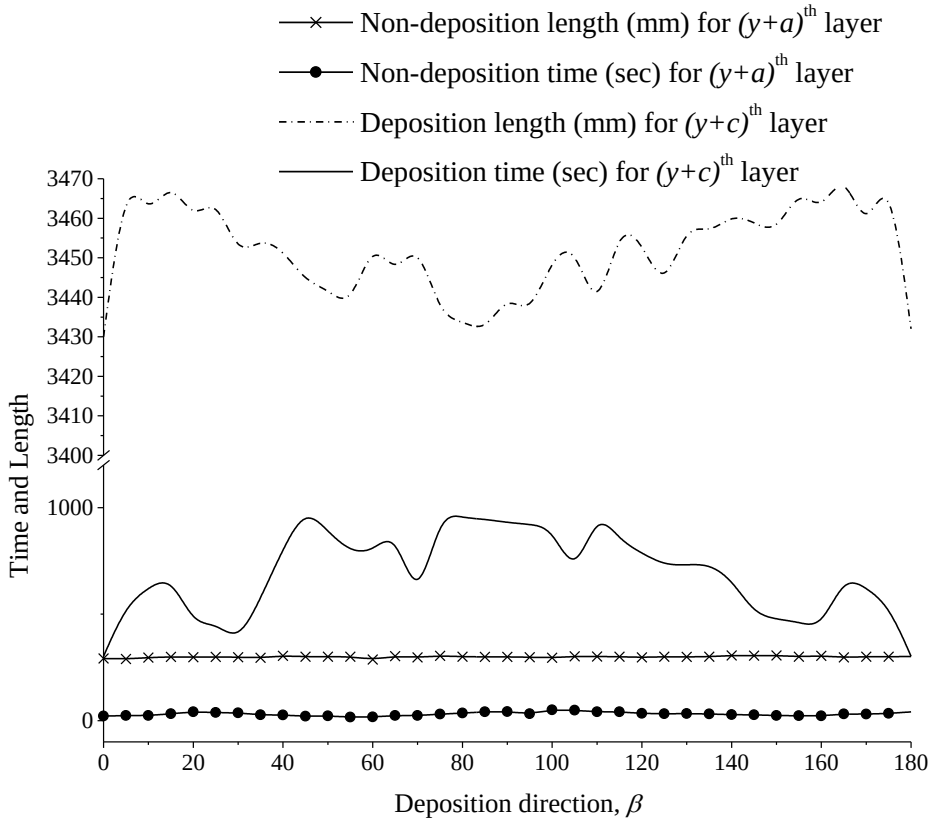

Figure 23. Deposition travel lengths for tool at different deposition directions for two layers of Example 1.

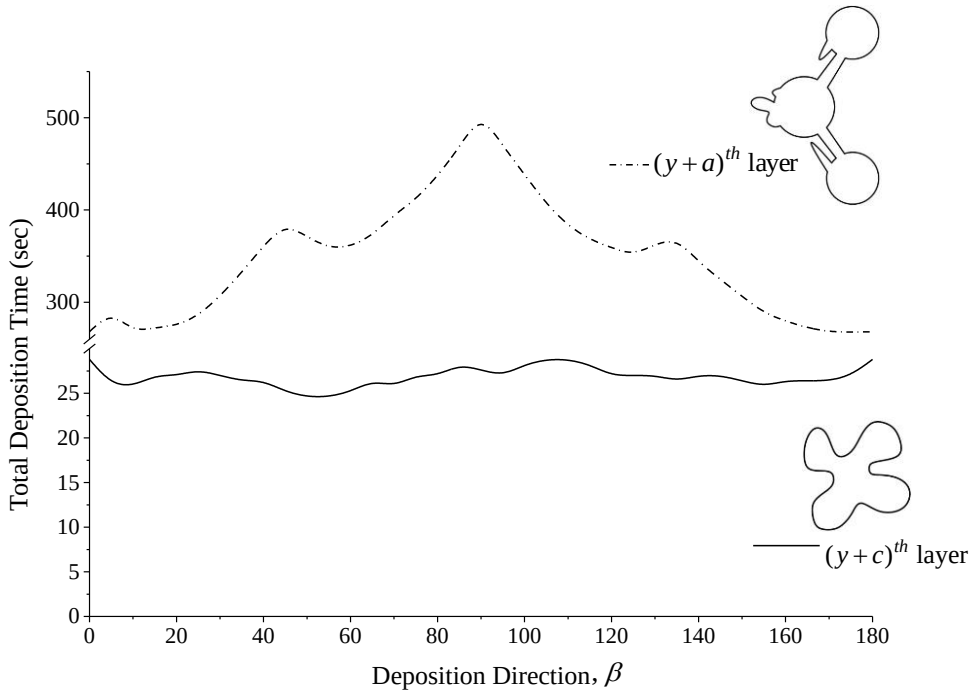

Figure 24. Total layer deposition time at different deposition directions for two layers of Example 1.

For Example 2, the non-deposition times for five arbitrarily selected layers along different build directions and at different height locations are analyzed and the results are shown in Figure 25. Because of the nature of these arbitrary slices, their non-deposition times remain low along 60° to 120° angle range. However, these non-deposition times can increase significantly along some directions which is depicted in Figure 25. The proposed methodology is also compared with two existing methodologies found in literature and shown in Table 4. The proposed methodology provides optimum deposition direction which has smaller objective function value and requires lower build time. Example 1 has higher shape complexity than Example 2 and shows significant improvement in the metrics.

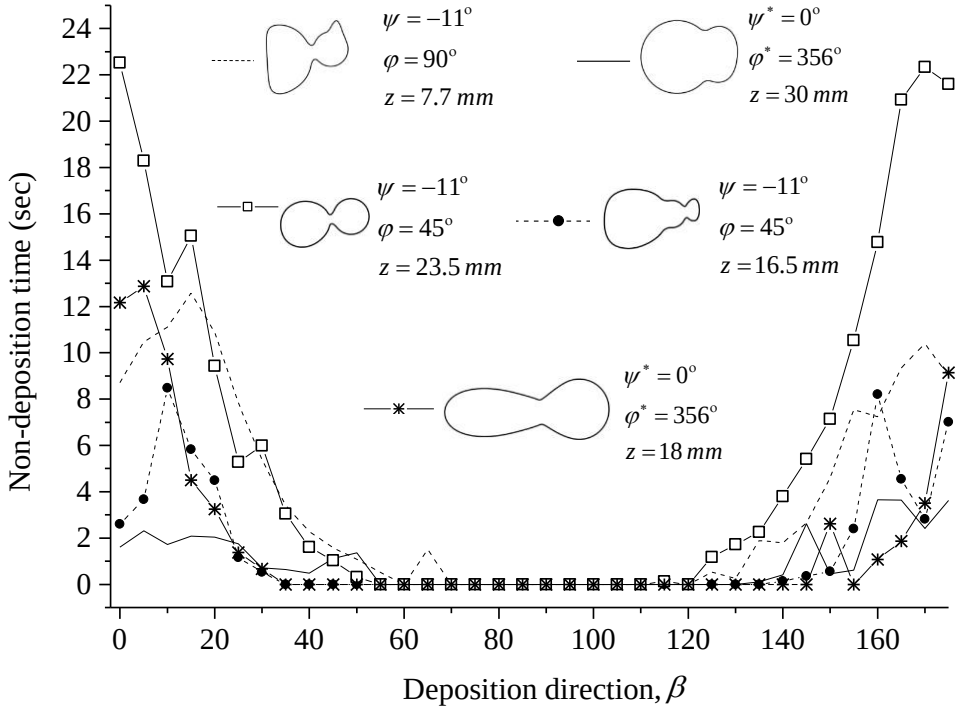

Figure 25. Non-Deposition times at different contours along different build directions of Example 2.

Table 4. Comparison between proposed methodology and existing methodologies from literature

	Example 1			Example 2		
	Build time (min)	Objective Function Value	ψ^*, φ^*	Build time (min)	Objective Function Value	ψ^*, φ^*
Proposed Methodology	306	0.197	11°, 304°	89	0.126	0°, 356
Thrimurthulu *et al.* [5]	368	0.444	–50°, 70°	95	0.341	0°, 90°
Byun and Lee [9]	353	0.310	10°, 100°	91	0.226	0°,0°

4.3. Remarks

Both fabrication discontinuity and complexity is quantified in the objective function to measure to determine material deposition orientation considering the resource requirement. The two stage optimization methodology reduces the overall resource consumption during the value added part building processes. However, the effect of the optimal build direction is carried into the toolpath planning stage since the layer geometry changes with the change in build orientation. Also the thin layer features of intricate parts may introduce fabrication complexity for material deposition. Hence, a combined framework for simultaneous determination of build orientation and toolpath direction based on geometric complexity is proposed in the next Section.

5. GEOMETRIC ATTRIBUTE DRIVEN CONCURRENT PROCESS PLAN FOR AM

Part attributes such as surface quality [1-15], accuracy [16], volumetric [17-20] errors, support volume [2, 6, 21], and build time [2, 3, 5, 8-12, 15-17] are often used to determine the optimum build direction. Similarly, deposition direction for zigzag tool-path was optimized mostly for layer build time [15, 22, 23], the number of turns [24], and tool start-stops [15, 23, 25]. Thus far, either build direction or tool-path direction is optimized independently considering one or multiple attributes in the objective function. In case of multiple attributes, normalized weights are commonly assigned to the respective attributes, where the weights are chosen arbitrarily [5, 9, 10, 13], by experience [34], or taken as user defined input [21]. However, different sets of weights in multi-attribute decision making process can generate diverse results. The arbitrary or non-systematic selection of weights could be the main downside of such assessment process [47, 50]. Thus, determining the part attribute weights with decision theory principle can standardize or align the design process and segregate it from experience. Furthermore, optimizing either build direction or tool-path direction undermines the hierarchical relationship in the AM process plan and may generate sub-optimal solution. Both build direction and tool-path direction alter the layer topology and tool-path pattern, which eventually determine the process and part attributes. But, the geometry is not taken into consideration while determining the build and tool-path orientations.

In this section, an integrated framework is proposed to concurrently determine the optimum build orientation and tool-path/deposition/scanning direction using the Hypothetical Equivalents and Inequivalents Method (HEIM) and a Genetic Algorithm (GA). Seven part geometric attributes– slenderness index, width index, depth index, object fill index, discontinued area index, layer aspect ratio, and layer fill index are measured and assimilated to their linear

weighted sum in the proposed model. The weights associated with these seven geometric attributes reflect their relative importance. HEIM is used to determine the appropriate weights of the geometric attributes. The proposed methodology is designed on the basis of the geometries and attributes of parts to ensure manufacturability and minimize fabrication complexity in AM processes. An exhaustive search method would require extensive computational resources even for a coarse resolution/increment of the rotation angles. An evolutionary algorithm such as GA can be effective in solving the current AM process planning problem. The proposed work will maximize the surface area and reduce thin/irregular features in each layer which may directly affect the fabrication time in general AM processes with or without synthetic support. Furthermore, the findings can certainly be helpful for multi-head/multi-beam deposition and non-deposition based AM processes. The roadmap of the proposed methodology is shown in Figure 26.

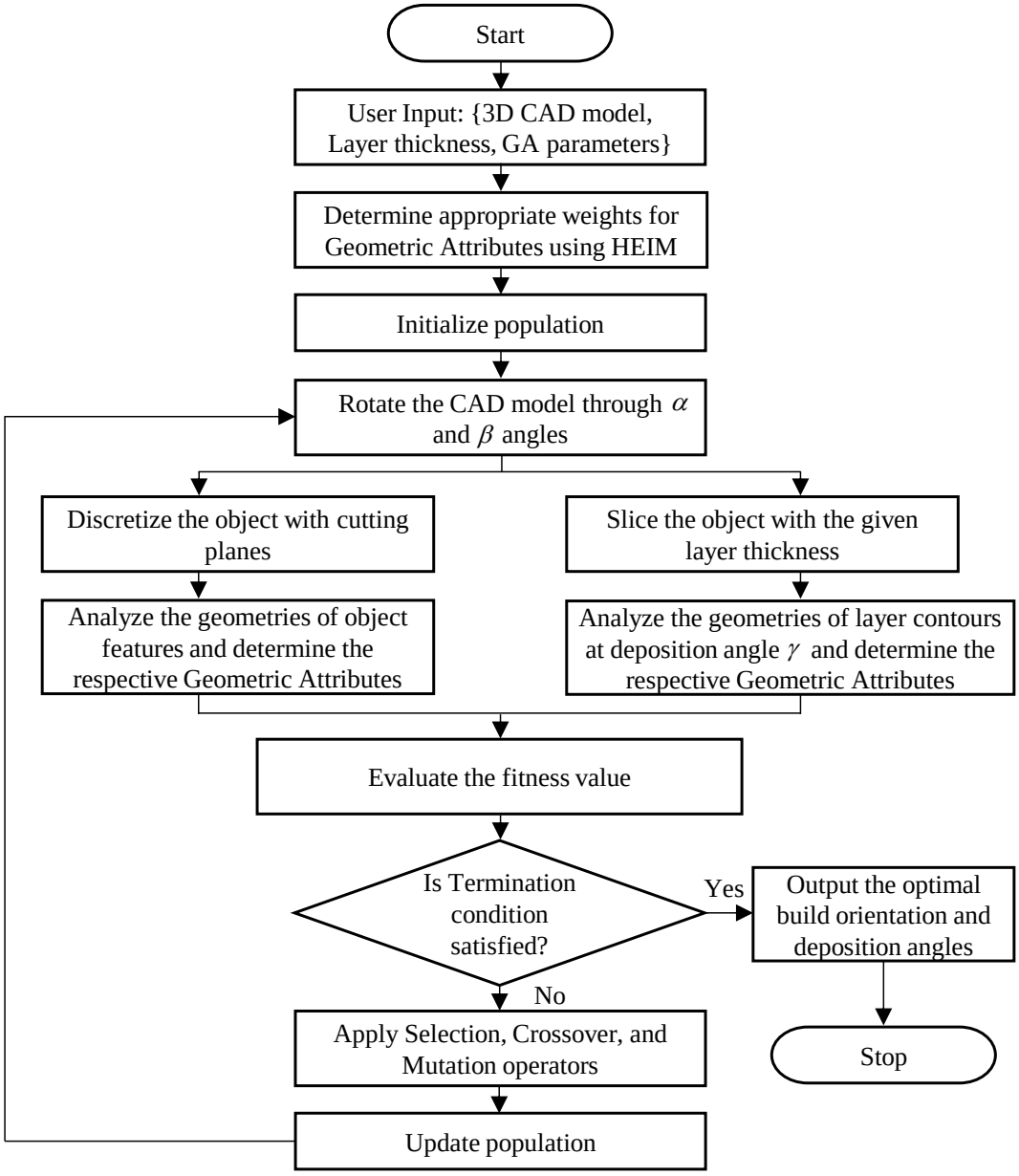

Figure 26. Proposed GA based approach to concurrently determining build orientation and tool-path direction.

5.1. Part Attributes and Geometry

In layer manufacturing, layers are generated by slicing the object with a set of parallel planes perpendicular to build direction. Materials are cured or deposited within the layer boundaries in consecutive order and stacking these layers one upon another creates the fabricated part. The process can be continuous or discrete depending upon the layer topology which may

affect both part and process attributes. The layer contours generated from the slender and concave features of an object can introduce frequent changes in tool-path direction and increased tool start-stops and non-deposition/non-curing travel of tool, which can lead to fabrication complexity [15, 25, 51]. Build direction, which is measured with angles α and β, can significantly alter the layer topology. By tailoring the build orientation, the slender, small sized, and concaved shaped layer features can be avoided. Moreover, with appropriate tool-path direction (γ), the effect of layer concavity on the process attributes can further be alleviated. In this section, the geometry of an object is analyzed through seven attributes including slenderness index ($I_{O,1}$), width index ($I_{O,2}$), depth index ($I_{O,3}$), object fill index ($I_{O,4}$), discontinued area index ($I_{L,1}$), layer aspect ratio ($I_{L,2}$), and layer fill index ($I_{L,3}$). Among them, the first four attributes measure the contribution of build orientation to the layer geometry and the rest measure the effect of tool-path direction contributed by the layer features.

5.1.1. Object Geometric Attributes

The slenderness index captures the inconsistency between the width and depth of object features. A lower slenderness index means that the widths and depths of the object features are almost equal, which is apparently desirable. The effect of slender features can be minimized by reducing the slenderness index through leveraging build orientation and tool-path direction. For instance, the object shown in Figure 27(a) has slender features in its upper and lower sections. The layers generated from this feature would have higher slenderness index and may bring undesirable part attributes. On the other hand, a different build orientation of the same object as shown in Figure 27(b) results in layers with uniform slenderness index. For both build orientations, the surface quality and build time are measured and shown in Table 5. The surface quality can be measured by comparing the facets' normal with the build vector. The stair case

effect can be quantified with the measured angle for both instances and the methodology is discussed in Section 3.1.3. On the other hand, fabrication time is measured using two commercially available software (CURA [52] and Stratasys Insight [53]). For the same orientation, the build time measured is proportional but different due to the difference in material deposition rate.

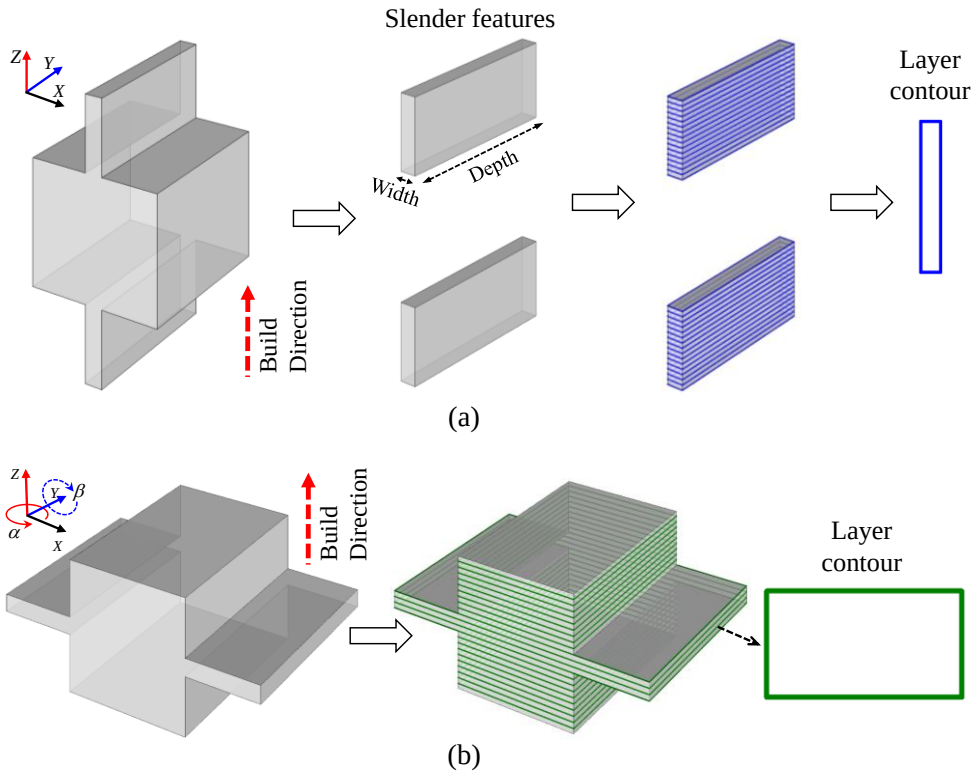

Figure 27. Effect of build orientation on the layer geometry of slender features

Table 5. Part attribute values for two different build orientations of the objects shown in Figure 27, Figure 28, and Figure 29.

Object and Orientation	Surface quality factor	Estimated time by CURA [52] (in min)	Estimated time by Stratasys Insight [53] (in min)
Figure 27(a)	0	22	42
Figure 27(b)	0	20	36
Figure 28(a)	0.1627	38	58
Figure 28(b)	0.2541	34	49
Figure 29(a)	0.5858	37	45
Figure 29(b)	0.2887	27	41

Similarly, when both width and depth of the layer features are noticeably small, the process may be equally challenged and may cause difficulties in material deposition/curing. This can even happen to the features with good slenderness index. Figure 28 is a conceptual illustration of how choosing appropriate build orientation can help minimize the effect of this type of object feature. The object shown in Figure 28(a) generates some tiny layers. By changing its build orientation as shown in Figure 28(b), layers with better width and depth indices can be achieved. The same process attributes (i.e., time and surface quality) are measured for this object and the results are shown in Table 5. Even though, the surface quality attribute is superior in Figure 28(a), the fabrication time required is lower for Figure 28(b).

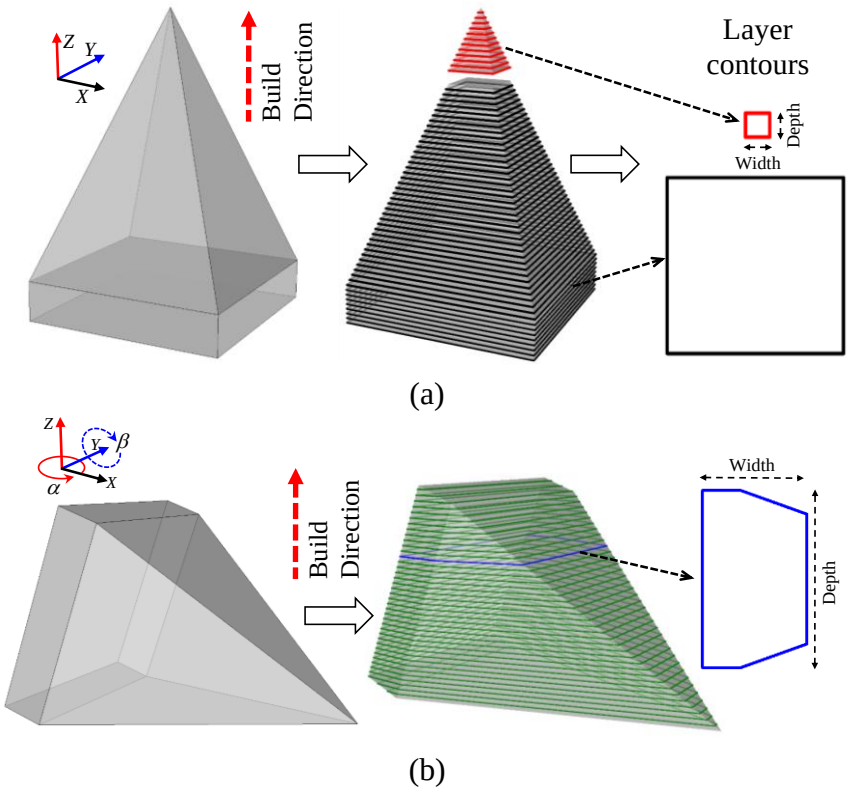

Figure 28. Effect of build orientation on considerably small sized layers.

The geometry of an object can also be analyzed with the object fill index, which can be measured by taking the ratio of each object feature's volume to its rectilinear bounding box. An

object feature with the higher object fill index may generate geometrically uniform layers with good attributes. However, a change in build orientation/direction may change the object fill index for the same object. For example, the object shown in Figure 29(a) poorly fills its bounding box. Rotating the object with a different orientation, shown in Figure 29(b), results in a better object fill index. The same process attributes (i.e., time and surface quality) are measured for this object and the results are shown in the Table 5. For both instances, Figure 29(b) demonstrates a desirable result.

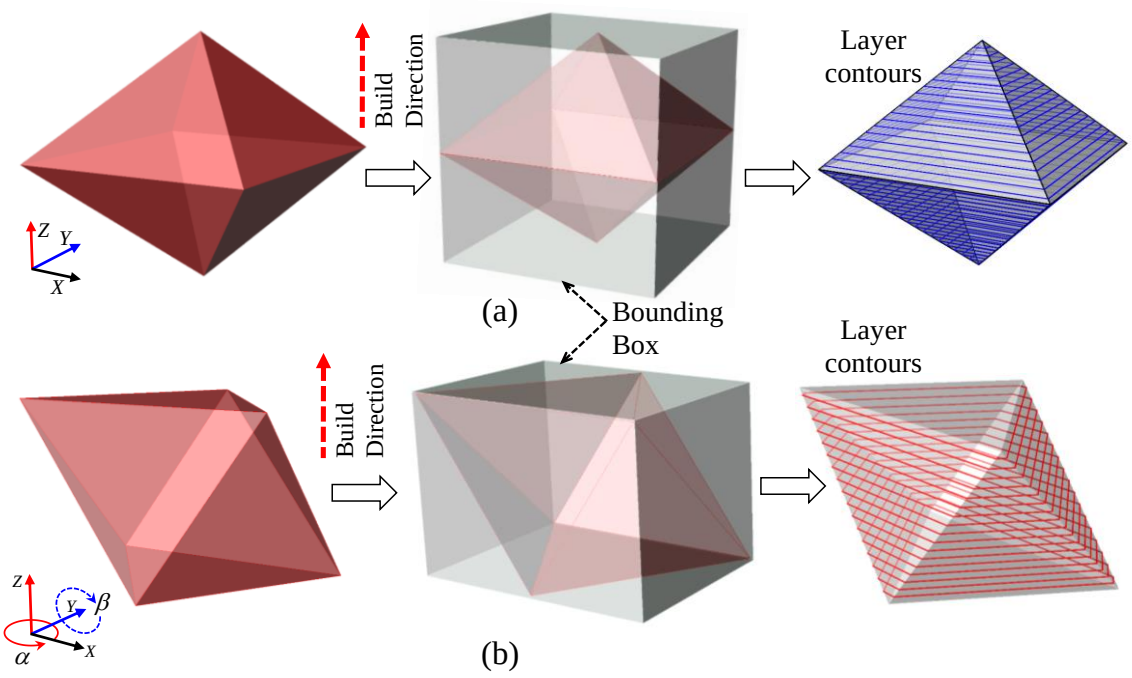

Figure 29. Interaction between build orientation and object fill index

5.1.2. Layer/Slice Geometric Attributes

Analyzing the layer geometry is also important to identify its effect on process and part attributes. The concave feature in layers can cause more tool start-stop, change in tool-path direction, and air travel which can lead to fabrication complexity. Depending on the layer geometry, the effect of concave features can be reduced by altering the tool-path direction/angle (γ). Discontinued area index can be introduced to quantify the concave layer features. The tool-

path direction pair 45º–135º shown in Figure 30(a) results in some discontinuous features and material cannot be deposited continuously. If the tool-path directions are changed to 0º–90º for the same consecutive layers, 90º will lead to fully continuous tool-path on one layer and 0º will generate only one discontinuous segment as shown in Figure 30(b).

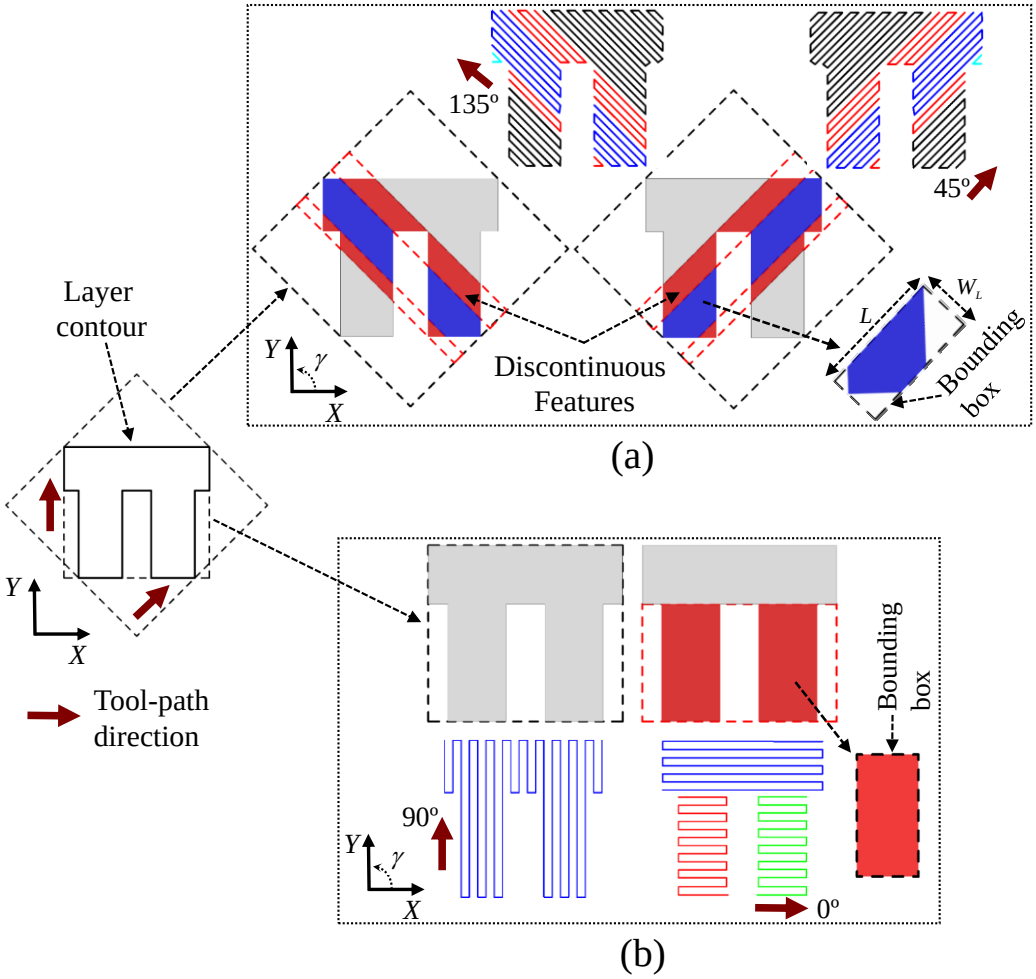

Figure 30. Interaction between tool-path direction and layer geometric attributes. (a) 45º–135º and (b) 0º–90º tool-path directions.

Furthermore, discontinuous features in concave layers will have undesirable short toolpath segments as shown in Figure 30(a). However, a relatively longer tool-path segment can be achieved for a discontinuous feature having better aspect ratio as shown in Figure 30(b). Often time, the layer aspect ratio may not reflect the actual shape of the discontinuous feature as

shown in Figure 30(a). Layer fill index can analyze how much the layer features fill their bounding boxes. For the 0º–90º crisscross tool-path demonstrated in Figure 30(b), tool-path direction at 0º generates a discontinuous feature with better layer fill index. Thus, both build direction and tool-path direction alter the layer topology and tool-path pattern which implicitly affect the part and process attributes. The framework proposed in this section quantifies their combined effect on the part and process attributes by analyzing the generated geometry.

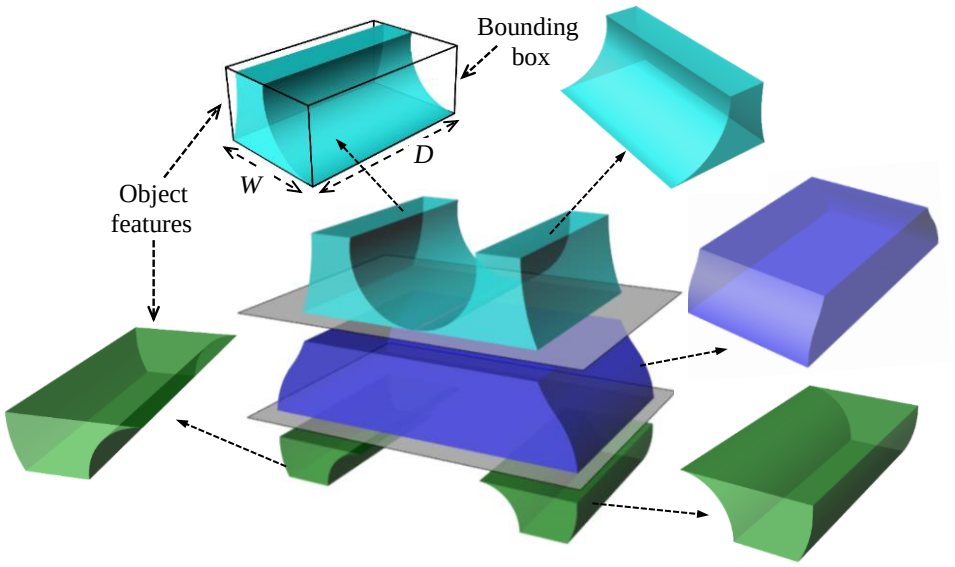

Figure 31. Object discretized with parallel planes and bounding box construction for one of the object features.

To implement the proposed methodology, a 3D object is first discretized into features with a set of parallel planes as shown in Figure 31. The planes are generated by analyzing the object geometry and the change in curvatures [15]. Once discretized, the features' attributes are quantified to construct the objective function. The seven geometric attributes discussed above are measured where the first four among them are formulated by Eq. (24). The rest are formulated by Eq. (25).

$$\mathbf{I}_O = \left[I_{O,1} = \left(1 - \frac{W}{D}\right),\ I_{O,2} = \left(\frac{T}{W+T}\right),\ I_{O,3} = \left(\frac{T}{D+T}\right),\ I_{O,4} = \left(1 - \frac{V}{V_B}\right) \right] \tag{24}$$

$$\mathbf{I}_L = \left[I_{L,1} = \left(\frac{A_D}{A} \right),\ I_{L,2} = \left(1 - \frac{W_L}{L} \right),\ I_{L,3} = \left(1 - \frac{A}{A_B} \right) \right] \tag{25}$$

where, $\mathbf{I}_O$ and $\mathbf{I}_L$ are the geometric attribute vectors corresponding to build orientation and tool-path direction, respectively. V is the volume of a discretized object-feature and D, W, and V_B are the depth, width, and volume of the discretized object-feature's bounding box, respectively, as shown in Figure 31. T is defined as the threshold dimension based on the fabrication process. A_D and A are the areas of discontinuous layer-feature and the entire layer, respectively. L, W_L, and A_B are the length, width, and area, respectively, of the bounding box of a discretized layer feature as shown in Figure 30. Here, $L \geq W_L$. Each of the geometric attribute entries in Eqs. (1) and (2) is normalized such that they all vary between 0 and 1.

Considering their importance, a normalized weight is assigned to each of these attributes in Eq. (24) and (25). These weights are optimized using HEIM. Considering the weight factors, objective function is formulated as $f(\alpha, \beta, \gamma) = \mathbf{w}_O \mathbf{I}_O^T + \mathbf{w}_L \mathbf{I}_L^T$, which is a function of build orientation angles (α, β) and tool-path angle (γ). Here, $\mathbf{w}_O = \{w_{O,m}\}_{m=1,2,3,4.}$ are the weights assigned to the four geometric attributes of Eq. (24), and $\mathbf{w}_L = \{w_{L,n}\}_{n=1,2,3.}$ are the weights assigned to the three geometric attributes of Eq. (25). The attribute weights are determined using hypothetical equivalents and inequivalents method (HEIM) [47] discussed in Section 5.2. A $\gamma \pm \varepsilon$ crisscross filling pattern is employed, where tool-path angles for odd numbered layers would be $\gamma_{odd} = \gamma$ and for even numbered layers would be $\gamma_{even} = \gamma + \varepsilon$ or $\gamma_{even} = \gamma - \varepsilon$. The analytical model, represented by Eq. (26), is formulated as a minimization problem to concurrently determine both optimum build orientation and tool-path direction.

$$
\begin{aligned}
&\text{Min } f(\alpha,\beta,\gamma) = \mathbf{w}_O\,\mathbf{I}_O{}^{\mathrm{T}} + \mathbf{w}_L\,\mathbf{I}_L{}^{\mathrm{T}} \\
&\text{s.t.} \\
&90° \le \alpha \le 270°, \\
&0° \le \beta \le 360°, \\
&0° \le \gamma \le 180°, \\
&\gamma_{odd} = \gamma, \quad \gamma_{even} = \gamma \pm \varepsilon, \\
&w_{O,m} \in \mathbf{w}_O, \quad m = 1,2,3,4. \\
&w_{L,n} \in \mathbf{w}_L, \quad n = 1,2,3.
\end{aligned}
\tag{26}
$$

This function varies as the object is rotated about *Z* and *Y* axes by angles α and β, respectively, and the tool-path direction is rotated about *Z* axis by angle γ in a standard 3D coordinate system.

5.2. Weight Determination

In this work, the hypothetical equivalents and inequivalents method (HEIM) [47] is used to determine the appropriate weights assigned to the geometric attributes introduced in the objective function of Eq. (26). HEIM is mathematically sound and can determine the actual importance of the attributes using a set of preferences stated by a decision maker rather than choosing weights arbitrarily from experience or intuition. In this technique, the user preferences are used to determine the weights of the geometric attributes. For each attribute, the weight becomes the variable and a set of outcomes is selected as hypothetical alternatives. The user provides both equality and inequality preferences among the hypothetical alternatives, which are used to determine the optimum weight values.

In this thesis, hypothetical alternatives are defined as the pairs of hypothetical build orientation and tool-path orientation (α,β,γ). The user preference between two hypothetical alternatives can be used to form a constraint. Thus, a set of constraints is formulated from the preference information among all the hypothetical alternatives as shown in Eq. (27). The objective function in Eq. (27) ensures the summation of all the weight values is unity. Solving Eq. (7) yields the optimum values of the attribute weights.

$$
\begin{aligned}
&\text{Min } \; [1-(\sum_{m=1}^{4} w_{O,m} + \sum_{n=1}^{3} w_{L,n})]^2 \\
&\text{s.t.} \\
&f(\alpha,\beta,\gamma)_i - f(\alpha,\beta,\gamma)_j \le -\delta; \quad i, j = 1,2,\text{K}\ , a \text{ and } i \ne j \\
&0 \le w_{O,m} \le 1; \quad \forall m \\
&0 \le w_{L,n} \le 1; \quad \forall n
\end{aligned} \tag{27}
$$

Here, $f(\alpha,\beta,\gamma)_i$ and $f(\alpha,\beta,\gamma)_j$ are the values of i^{th} and j^{th} hypothetical alternatives, respectively. These values can be determined using the objective function of Eq. (26). The constraints are formulated considering i^{th} hypothetical alternative is preferred to j^{th} hypothetical alternative. δ is a small positive number, which is used to ensure the inequality between two hypothetical alternatives.

A set of hypothetical build orientation and tool-path direction pairs $\{P_i = (\alpha,\beta,\gamma)_i\}$ are created using a 2^{7-3} fractional factorial experimental design [54] as there are seven attributes and each attribute is assumed to have two levels, low (0) and high (1). Here, the low level (0) is the preferred level for all attributes of the hypothetical alternatives. Note that all the geometric attributes in Eq. (26) are normalized and as a result, the actual attribute values are ranging from 0 to 1. Table 6 shows the corresponding attribute levels and the overall values of the hypothetical build orientation and tool-path direction pairs.

Table 6. Attribute levels and overall values of the hypothetical alternatives.

Hypothetical alternatives (P_i)	Geometric attributes							Values $(f(P_i))$
	$I_{O,1}$	$I_{O,2}$	$I_{O,3}$	$I_{O,4}$	$I_{L,1}$	$I_{L,2}$	$I_{L,3}$	
P_1	0	0	0	0	0	0	0	0
P_2	1	0	0	0	1	0	1	$w_{O,1}I_{O,1} + w_{L,1}I_{L,1} + w_{L,3}I_{L,3}$
P_3	0	1	0	0	1	1	0	$w_{O,2}I_{O,2} + w_{L,1}I_{L,1} + w_{L,2}I_{L,2}$
P_4	1	1	0	0	0	1	1	$w_{O,1}I_{O,1} + w_{O,2}I_{O,2} + w_{L,2}I_{L,2} + w_{L,3}I_{L,3}$
P_5	0	0	1	0	1	1	1	$w_{O,3}I_{O,3} + w_{L,1}I_{L,1} + w_{L,2}I_{L,2} + w_{L,3}I_{L,3}$
P_6	1	0	1	0	0	1	0	$w_{O,1}I_{O,1} + w_{O,3}I_{O,3} + w_{L,2}I_{L,2}$
P_7	0	1	1	0	0	0	1	$w_{O,2}I_{O,2} + w_{O,3}I_{O,3} + w_{L,3}I_{L,3}$
P_8	1	1	1	0	1	0	0	$w_{O,1}I_{O,1} + w_{O,2}I_{O,2} + w_{O,3}I_{O,3} + w_{L,1}I_{L,1}$
P_9	0	0	0	1	0	1	1	$w_{O,4}I_{O,4} + w_{L,2}I_{L,2} + w_{L,3}I_{L,3}$
P_{10}	1	0	0	1	1	1	0	$w_{O,1}I_{O,1} + w_{O,4}I_{O,4} + w_{L,1}I_{L,1} + w_{L,2}I_{L,2}$
P_{11}	0	1	0	1	1	0	1	$w_{O,2}I_{O,2} + w_{O,4}I_{O,4} + w_{L,1}I_{L,1} + w_{L,3}I_{L,3}$
P_{12}	1	1	0	1	0	0	0	$w_{O,1}I_{O,1} + w_{O,2}I_{O,2} + w_{O,4}I_{O,4}$
P_{13}	0	0	1	1	1	0	0	$w_{O,3}I_{O,3} + w_{O,4}I_{O,4} + w_{L,1}I_{L,1}$
P_{14}	1	0	1	1	0	0	1	$w_{O,1}I_{O,1} + w_{O,3}I_{O,3} + w_{O,4}I_{O,4} + w_{L,3}I_{L,3}$
P_{15}	0	1	1	1	0	1	0	$w_{O,2}I_{O,2} + w_{O,3}I_{O,3} + w_{O,4}I_{O,4} + w_{L,2}I_{L,2}$
P_{16}	1	1	1	1	1	1	1	$w_{O,1}I_{O,1} + w_{O,2}I_{O,2} + w_{O,3}I_{O,3} + w_{O,4}I_{O,4}$ $w_{L,1}I_{L,1} + w_{L,2}I_{L,2} + w_{L,3}I_{L,3}$

In Table 6, all the geometric attribute values of hypothetical alternative P_1 are zero indicating that P_1 is highly preferable in the minimization problem. Each alternative is defined with the contribution of attributes. For example, between alternatives P_2 and P_3, P_2 can be characterized with the following attributes– width index ($I_{O,2}$) and layer aspect ratio ($I_{L,2}$) at

the desired level (0); and slenderness index ($I_{O,1}$) and layer fill index ($I_{L,3}$) at the undesired level (1). Once characterized, the preference between alternatives needs to be determined by the user. For instance, if attributes $I_{O,2}$ and $I_{L,2}$ are more desirable than attributes $I_{O,1}$ and $I_{L,3}$, then the preference relationship between alternatives P_2 and P_3 can be defined as $P_2 \pi P_3$, where "π" means "preferred to". The constraint will be developed between P_2 and P_3 as $f(P_2) - f(P_3) \le -\delta$. Similarly, for preferences among three alternatives, three constraints can be developed. Thus, the following preference relations among the hypothetical alternatives listed in Table 6 can be developed using the information given in same table: $P_1 \pi P_2 \pi P_3$, $P_6 \pi P_5 \pi P_4$, $P_8 \pi P_7$, $P_8 \pi P_9$, $P_{10} \pi P_{12} \pi P_{11}$, $P_{13} \pi P_{15}$, $P_{14} \pi P_{16}$. Finally, all the constraints in the minimization problem shown by Eq. (28) are formulated from these preference relations. By solving Eq. (28), the optimum values of the attribute weights can be determined.

$$
\begin{aligned}
&\text{Min} \quad [1-(\sum_{m=1}^{4} w_{O,m} + \sum_{n=1}^{3} w_{L,n})]^2 \\
&\text{s.t.} \\
&-w_{O,1} - w_{L,1} - w_{L,3} \le -\delta \\
&-w_{O,2} - w_{L,1} - w_{L,2} \le -\delta \\
&w_{O,1} - w_{O,2} - w_{L,2} + w_{L,3} \le -\delta \\
&-w_{O,1} - w_{O,2} + w_{O,3} + w_{L,1} \le -\delta \\
&-w_{O,2} + w_{O,3} - w_{L,3} \le -\delta \\
&w_{O,1} - w_{L,1} - w_{L,3} \le -\delta \\
&w_{O,1} + w_{O,2} + w_{O,3} - w_{O,4} + w_{L,1} - w_{L,2} - w_{L,3} \le -\delta \\
&w_{O,1} + w_{L,1} - w_{L,3} \le -\delta \\
&w_{O,1} - w_{O,2} + w_{L,2} - w_{L,3} \le -\delta \\
&-w_{O,2} + w_{L,1} + w_{L,2} \le -\delta \\
&-w_{O,2} + w_{L,1} - w_{L,2} \le -\delta \\
&0 \le w_{O,m} \le 1; \quad \forall m \\
&0 \le w_{L,n} \le 1; \quad \forall n
\end{aligned}
\tag{28}
$$

5.3. Optimization with Genetic Algorithm

In an optimization process, classical exhaustive methods usually suffice for small solution spaces. However, for larger solution spaces, evolutionary heuristic methods may provide optimal or near optimal solutions in a relatively lower number of iterations. Genetic algorithm is one of the stochastic evolutionary search techniques which can be used to solve complex optimization problems [55]. GA imitates the process of evolution by natural selection and improves a randomly generated population of potential solutions by applying genetic operations, i.e., crossover and mutation [56]. The formulated problem in Eq. (26) contains three decision variable (α, β, γ) derived from build orientation and tool-path direction. The variables have infinite alternatives within their respective ranges and solving them concurrently will increase the solution space in an exponential manner. In this section, GA is used to determine the optimal build orientation and tool-path direction by solving the minimization problem formulated in Eq. (26).

In this section, the build orientation is represented by two rotation angles (α and β) of the object about Z and Y axes, respectively, in a standard 3D coordinate system. By changing the magnitudes of these two angles, any orientation in the 3D space can be achieved. Similarly, the tool-path direction is represented by a rotation angle γ about the vertical Z axis. Hence, the three independent decision variables α, β, and γ would constitute a chromosome/individual of the GA population. A binary string is used to encode these three variables as shown in Figure 32. Each chromosome consists of 34 bits where the first 11 bits encode α in the range of 90º–270º, the next 12 bits encode β in the range of 0º–360º, and the last 11 bits encode γ in the range of 0º–180º. Every single bit in a chromosome is called a gene. For the initial population of a specified size N, each of its chromosomes is randomly generated in this bitwise fashion. In each

generation, the binary encoded chromosomes are decoded into their real values to evaluate them. Selection, crossover, and mutation operators are then applied to generate new population.

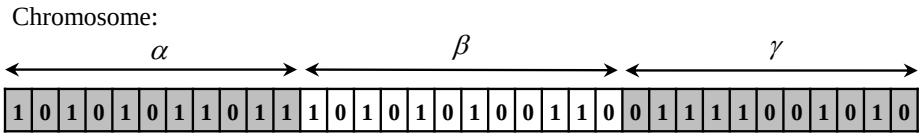

Figure 32. A binary encoded chromosome.

The values of GA parameters such as population size, crossover, and mutation probabilities influence the algorithm performance. A GA with efficient parameter values can converge and obtain optimum or near optimum solution in a reasonable number of iterations (computational time). Thus, without proper setting of GA parameters, it's very unlikely to achieve convergence and optimum solution. Tuning the GA parameters to an appropriate level can be done through studying how the performance of the GA depends on its parameter values. Therefore, a screening experiment on subsize population is performed for proper selection of the two main GA parameters, crossover probability $p_c \in [0,1]$ and mutation probability $p_m \in [0,1]$, from given sets of probability vectors. A grid search process is implemented for evaluation with respect to convergence rate, stability, and computational demands. The developed GA with various combinations of crossover and mutation probabilities is run on an object over a limited number of generations. The performance of the GA in this experiment is observed and the best parameter values are identified. The best crossover and mutation probabilities can be further investigated by incrementally varying them within their neighborhood space. Subsize population and limited number of generation are used in this experiment to reduce the computational effort.

5.4. Implementation

The proposed GA based methodology is implemented on two 3D example objects using a Visual Basic based script. All the computations are performed on a core i7 @3.6 GHz CPU with

8 GB RAM. The proposed methodology is utilized for extrusion based AM technique to determine the optimum build orientation and tool-path direction for the two distinct objects. The time required to implement the methodology on example 1 and example 2 are approximately 45 and 15 seconds per objective function evaluation, respectively. The GA input parameters defined by the user are population size, crossover probability, mutation probability, and generation limit. The crossover and mutation probabilities are selected through performing the screening experiment as discussed in Section 5.3. The maximum number of generation is used as the termination condition for GA. The GA parameter values used for both examples are listed in Table 7. In order to compare the effectiveness of GA, an exhaustive search method is also implemented for both examples, where α, β, and γ are incrementally varied by 10º, 10º, and 20º, respectively. These resolutions result in total 7030 iterations (objective function evaluations) for the given range of α, β, and γ The layer thickness is assumed 0.254 mm and for zigzag tool-path, ε in Eq. (26) is considered 90° for both objects.

The "Constrained Nonlinear Minimization" routine provided in MATLAB package is used to solve Eq. (28) for the optimum geometric attribute weights. It took about 8 seconds to compute the optimum attribute weights. To ensure the inequality between two alternatives in the constraints, $\delta = 0.01$ is considered. The following weight values of the geometric attributes determined by solving Eq. (28) are rounded to 2 decimal places and used in Eq. (26) for both examples: $w_{O,1} = 0.07$, $w_{O,2} = 0.18$, $w_{O,3} = 0.15$, $w_{O,4} = 0.25$, $w_{L,1} = 0.10$, $w_{L,2} = 0.08$, and $w_{L,3} = 0.17$. Both object fill index and layer fill index represent the void which in turn generates significant changes in deposition modalities. The depth and width indices determine to what extent the object features are small compared to a set threshold value. The weights corresponding to these four attributes comprise 75% of the total weight. Therefore, the weight values

determined using HEIM appropriately reflect the actual importance of the geometric attributes indicated by the preferences among the hypothetical alternatives given in Section 3.

Table 7. GA parameters.

Example 1	Example 2
Population size: 10	Population size: 60
Crossover probability: 0.6	Crossover probability: 0.6
Mutation probability: 0.01	Mutation probability: 0.01
Maximum number of generation: 50	Maximum number of generation: 60

Example 1, which is used to demonstrate the proposed methodology, is shown in Figure 33(a). The object has a volume of 56130 cubic mm. The optimum build orientation and tool-path angle obtained using the proposed algorithm for the Example 1 are $\alpha^* = 147.80°$, $\beta^* = 14.24°$, and $\gamma^* = 75.80°$ as shown in Figure 33(b) and 11. The real values of the angles obtained from GA are rounded to two decimal places. As $\varepsilon = 90°$, the optimum tool-path angles for odd numbered layers and even numbered layers are $\gamma^*_{odd} = 75.80°$ and $\gamma^*_{even} = 165.80°$, respectively.

Figure 35(a) illustrates the convergence of GA for example 1. It achieves the best objective function value (0.19109) within 19 generations, which is equivalent to 190 iterations. Since the fitness value is the evaluation measure of a chromosome (build orientation and tool-path angle), the chromosome with the minimum fitness value is the best solution of that generation. The best objective function value obtained using the exhaustive search method is 0.19647 which requires 7030 iterations for the given increment sizes of α, β, and γ as shown in Figure 35(b). However, finer increments in exhaustive search might provide the same or even better solution than GA but would require excessive computational resources.

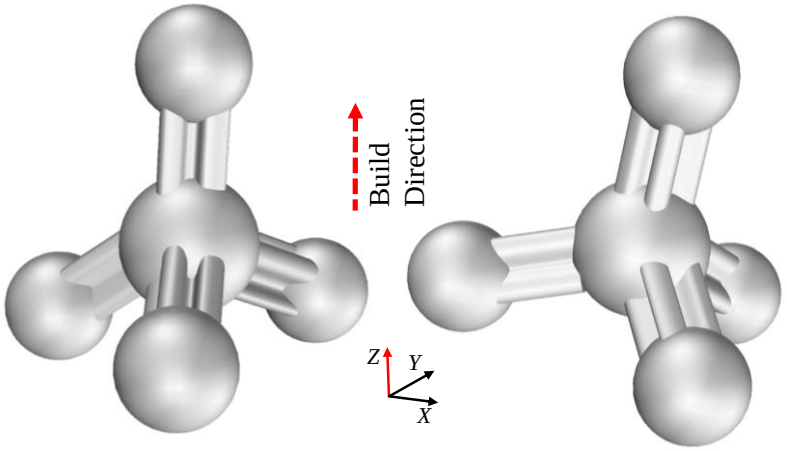

Figure 33. (a) Example 1 at reference orientation ($\alpha^* = 0°, \beta^* = 0°$) and (b) Example 1 at the optimal build orientation ($\alpha^* = 147.80°, \beta^* = 14.24°$).

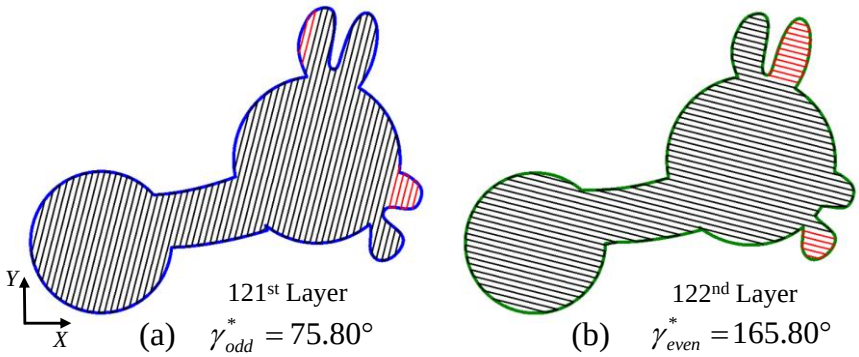

Figure 34. Optimum tool-path directions for odd and even numbered layers of example 1 at its optimum build orientation.

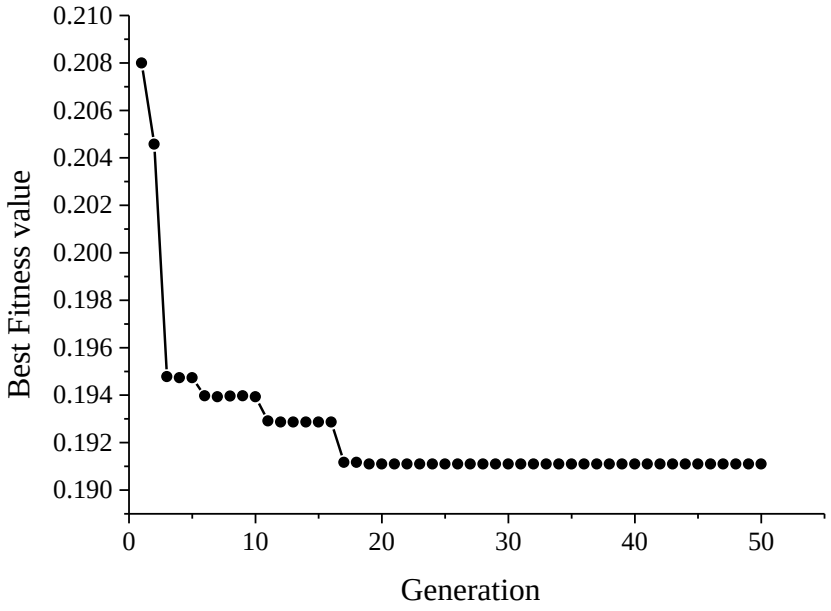

(a)

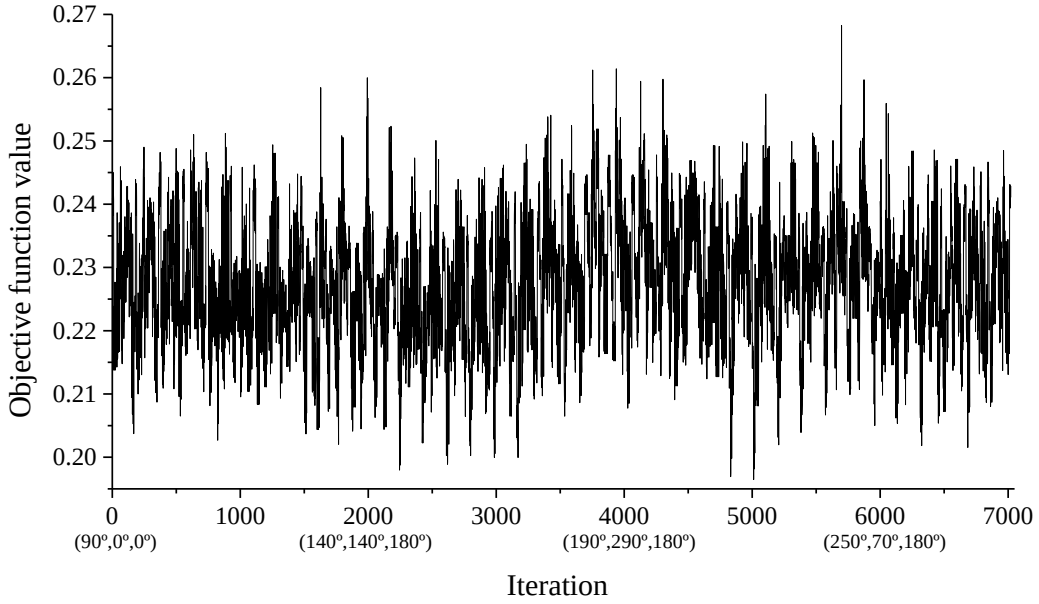

(b)

Figure 35. (a) Convergence plot of GA and (b) objective function vs. iteration plot of exhaustive method for Example 1.

The second example shown in Figure 36(a) is an earbud which has a volume of 3287 cubic mm. Using genetic algorithm, the optimum build orientation and tool-path angles obtained for the earbud are $\alpha^* = 91.67°$, $\beta^* = 269.45°$ and $\gamma^* = 75.8°$. Therefore, the optimum tool-path

angle for odd numbered layers and even numbered layers are $\gamma^*_{odd} = 75.8°$ and $\gamma^*_{even} = 165.8°$, respectively, as shown in Figure 37. The part oriented through α^* and β^* in the standard coordinate system is shown in Figure 36(b). The optimum build orientation results in minimum number of concave layer contours and the optimum tool-path angle further minimizes the overall contour discontinued area to approximately 3%, thereby reducing the undesired interruptions in tool movement. On the other hand, the reference orientation and tool-path angle $(\alpha = 0°, \beta = 0°, \gamma = 0°)$ experience concave contours with almost 12.4% overall discontinued area.

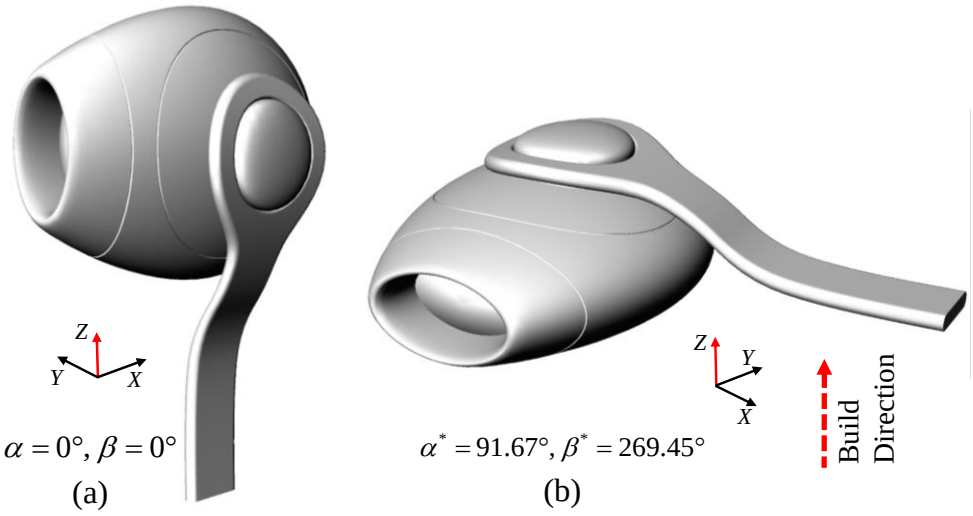

Figure 36. (a) Example 2 (earbud) at reference orientation ($\alpha^* = 0°, \beta^* = 0°$) and (b) Example 2 (earbud) at the optimal build orientation ($\alpha^* = 91.67°, \beta^* = 269.45°$).

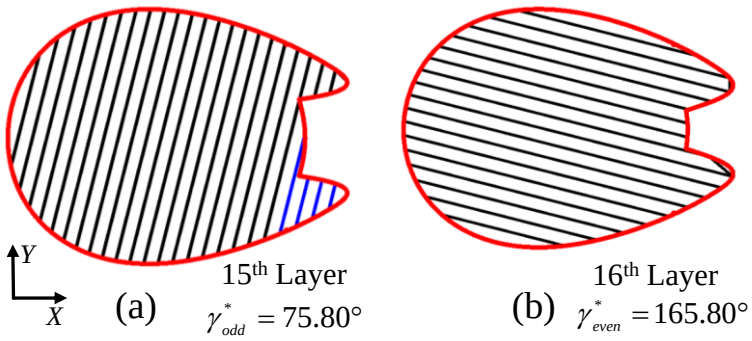

Figure 37. Optimum tool-path directions for odd and even numbered layers of the earbud at its optimum build orientation.

The GA for the earbud (example 2) converges to the minimum objective function value (0.20059) after 37 generations, which is equivalent to 2220 iterations as shown in Figure 38(a). On the other hand, the exhaustive method with the given increment sizes of α, β, and γ requires 7030 iterations and results in the minimum objective function value of 0.21556 as shown in Figure 38(b). During the grid based exhaustive search process, the ranges of α and β in Eq. (26) will generate the build directions in a 3D space of full sphere domain. As a result, the layer contours generated from the model will be symmetric among the first half and the second half of the α and β ranges. This phenomenon is exhibiting symmetry in the objective function value vs. (α, β, γ) plot as shown in both examples.

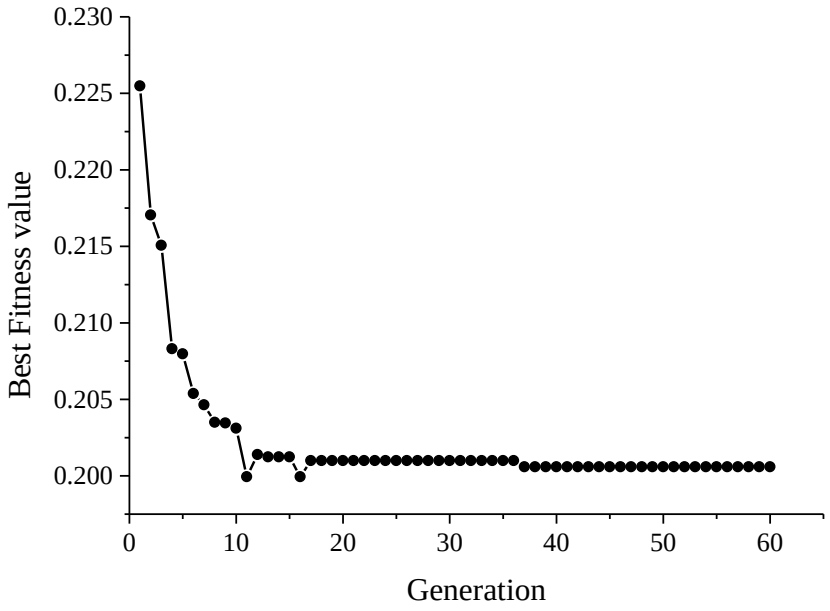

(a)

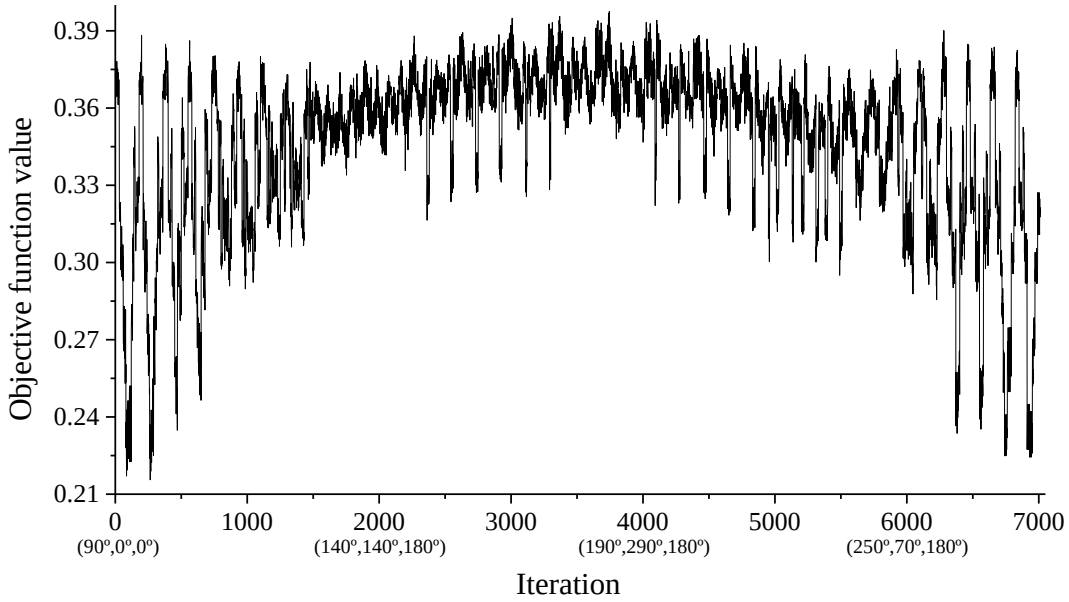

(b)

Figure 38. (a) Convergence plot of GA and (b) objective function vs. iteration plot of exhaustive method for Example 2.

To further assess the effectiveness of the proposed methodology, the total build times of both example parts are measured for different scenarios and shown in tation and tool-path direction.

Table 8. The time is measured using the build time estimation model from previous work [23] and the commercial FDM 3D printing software CURA [52]. The software uses its own tool-path direction and it cannot be changed by the user. Thus, build times corresponding to both optimum build orientation and tool-path direction cannot be collected from the software. For both parts, the optimum build orientation and tool-path angle yield minimum build time. Compared to example 1, the build time of example 2 corresponding to the optimum solution significantly improves. This happens because example 2 has more slender features which are reduced by adopting the optimum build orientation and tool-path direction.

Table 8. Build time comparison between optimum and arbitrary process plans.

Object	Build Orientation	Tool-path Direction	(α, β, γ)	Build Time (sec)	
				Time Estimation Model [23]	Commercial Software
Example 1	Optimum	Optimum	(147.80º, 14.24º, 75.80º)	9088	N/A
	Optimum	Arbitrary	(147.80º, 14.24º, 45º)	9206	13800
	Arbitrary	Optimum	(0º, 0º, 75.80º)	9139	N/A
	Arbitrary	Arbitrary	(0º, 0º, 30º)	9171	14100
Example 2	Optimum	Optimum	(91.67º, 269.45º, 75.80º)	420	N/A
	Optimum	Arbitrary	(91.67º, 269.45º, 0º)	444	900
	Arbitrary	Optimum	(0º, 180º, 75.80º)	587	N/A
	Arbitrary	Arbitrary	(0º, 180º, 0º)	578	1080

5.5. Remarks

Build orientation and tool-path direction are two important AM process parameters which are determined at the pre-processing stage of AM. Exhaustive search method would require extensive computational resources even for a coarse resolution/increment of the rotation angles. This fact justifies the use of GA to solve the current AM process planning problem. In this

section, a framework is developed for optimizing both build orientation and tool-path direction simultaneously by analyzing the 3D part geometry as well as the corresponding layer contours in order to minimize part fabrication complexity.

6. CONCLUSION AND FUTURE WORK

6.1. Conclusion

Build orientation and deposition direction are two important AM process parameters which are determined at the pre-processing stage of AM. Carefully determined build direction and deposition direction can significantly improve the process and fabrication attributes. In this thesis, a resource based build direction determination algorithm is proposed which considers contour plurality, geometric attributes, surface quality, build height. Various researches have proposed build direction algorithm for minimizing part quality, time, and support volume. However, multi contour layer requires more resources such as time, machine capability, and computational power which can be significant in case of free form objects. The proposed framework focuses on such areas and shows that it can reduce the number of multi-contour layers, thin features, and build height that may lead to lower part building time as well as lower fabrication complexity.

Then a toolpath path planning algorithm is also presented which minimizes deposition discontinuity for concave layer contours. Concave layer geometries which are very common for freeform objects introduce frequent tool start-stops causing substantial increase in build time. The proposed optimal toolpath reduces the effect of presence of concave features of layer geometries.

The build direction and deposition direction are usually optimized independently considering multiple attributes. However, such approach may sometimes produce sub-optimal solution due to the interdependency of the steps having hierarchical relationship in the AM process plan. Besides, both build direction and deposition direction alter the layer topology and tool-path pattern which eventually determine the process and part attributes. Therefore, in this

thesis, an integrated framework is proposed to concurrently determine the optimum build orientation and tool-path/deposition direction using Genetic Algorithm (GA). The proposed methodology is designed on the basis of the layer geometries and the resulting part attributes to ensure manufacturability and minimize fabrication complexity for parts in AM processes. The implementation of the algorithm free form shaped objects shows that the process converges within a reasonable number of iterations.

6.2. Future Work

Porous lattice/cellular structures consist of periodic or aperiodic arrangement of unit cells made of thin members. Therefore, slicing cellular structures generates numerous contour plurality as well as concave contours compared to nonporous objects. For example, a layer taken from the 2.5x5.5x2.5 mm cellular structure shown in Figure 39 contains so many small contours (see Figure 39(b)) which are very challenging to fabricate even with AM technologies. Such type of layers also result in weaker section in the fabricated part. This dramatically increased number of contours will require substantial resources during fabrication. Therefore, resource based process plan for cellular structures can be an interesting future research direction of this thesis.

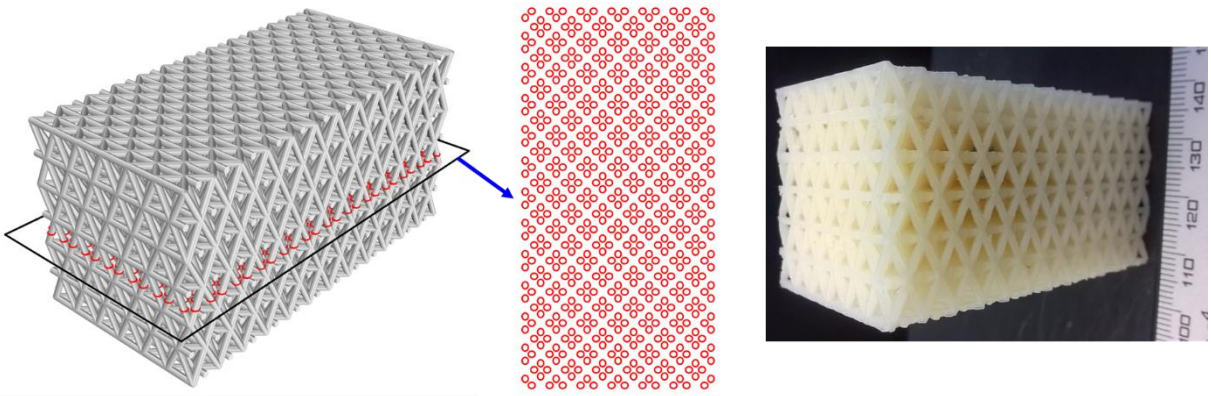

Figure 39. Cellular structure and contour plurality: (a) cellular structure block, (b) contours on a layer, and (c) fabricated structure.

REFERENCES

1. Alexander, P., S. Allen, and D. Dutta, *Part orientation and build cost determination in layered manufacturing.* Computer-Aided Design, 1998. **30**(5): p. 343-356.
2. West, A.P., S.P. Sambu, and D.W. Rosen, *A process planning method for improving build performance in stereolithography.* Computer-Aided Design, 2001. **33**(1): p. 65-79.
3. Ancău, M. and C. Caizar, *The computation of Pareto-optimal set in multicriterial optimization of rapid prototyping processes.* Computers & Industrial Engineering, 2010. **58**(4): p. 696-708.
4. Ahn, D., H. Kim, and S. Lee, *Fabrication direction optimization to minimize post-machining in layered manufacturing.* International Journal of Machine Tools and Manufacture, 2007. **47**(3–4): p. 593-606.
5. Thrimurthulu, K., P.M. Pandey, and N. Venkata Reddy, *Optimum part deposition orientation in fused deposition modeling.* International Journal of Machine Tools and Manufacture, 2004. **44**(6): p. 585-594.
6. Zhang, Y., et al., *Build orientation optimization for multi-part production in additive manufacturing.* Journal of Intelligent Manufacturing, 2015: p. 1-15.
7. Danjou, S. and P. Koehler, *Determination of Optimal Build Direction for Different Rapid Prototyping Applications*, in *Proceedings of the 14th European Forum on Rapid Prototyping*. 2009: Paris.
8. Byun, H.S. and K.H. Lee, *Determination of the optimal part orientation in layered manufacturing using a genetic algorithm.* International Journal of Production Research, 2005. **43**(13): p. 2709-2724.

9. Byun, H.-S. and K.H. Lee, *Determination of the optimal build direction for different rapid prototyping processes using multi-criterion decision making.* Robotics and Computer-Integrated Manufacturing, 2006. **22**(1): p. 69-80.

10. Canellidis, V., J. Giannatsis, and V. Dedoussis, *Genetic-algorithm-based multi-objective optimization of the build orientation in stereolithography.* The International Journal of Advanced Manufacturing Technology, 2009. **45**(7-8): p. 714-730.

11. Nikhil, P. and D. Kalyanmoy, *Multi-objective optimisation and multi-criteria decision making in SLS using evolutionary approachesnull.* Rapid Prototyping Journal, 2011. **17**(6): p. 458-478.

12. Pandey, P.M., K. Thrimurthulu, and N.V. Reddy, *Optimal part deposition orientation in FDM by using a multicriteria genetic algorithm.* International Journal of Production Research, 2004. **42**(19): p. 4069-4089.

13. Phatak, A.M. and S.S. Pande, *Optimum part orientation in Rapid Prototyping using genetic algorithm.* Journal of Manufacturing Systems, 2012. **31**(4): p. 395-402.

14. Singhal, S.K., et al., *Optimum Part Deposition Orientation in Stereolithography.* Computer-Aided Design and Applications, 2005. **2**(1-4): p. 319-328.

15. Ahsan, A.M.M.N., M.A. Habib, and B. Khoda, *Resource based process planning for additive manufacturing.* Computer-Aided Design, 2015. **69**: p. 112-125.

16. Choi, S.H. and S. Samavedam, *Modelling and optimisation of Rapid Prototyping.* Computers in Industry, 2002. **47**(1): p. 39-53.

17. Tyagi, S.K., et al., *Optimal part orientation in layered manufacturing using evolutionary stickers-based DNA algorithm.* Virtual and Physical Prototyping, 2007. **2**(1): p. 3-19.

18. Rattanawong, W., S.H. Masood, and P. Iovenitti, *A volumetric approach to part-build orientations in rapid prototyping.* Journal of Materials Processing Technology, 2001. **119**(1–3): p. 348-353.

19. Masood, S.H., W. Rattanawong, and P. Iovenitti, *A generic algorithm for a best part orientation system for complex parts in rapid prototyping.* Journal of Materials Processing Technology, 2003. **139**(1–3): p. 110-116.

20. Li, Y. and J. Zhang, *Multi-criteria GA-based Pareto optimization of building direction for rapid prototyping.* The International Journal of Advanced Manufacturing Technology, 2013. **69**(5-8): p. 1819-1831.

21. Paul, R. and S. Anand, *Optimization of layered manufacturing process for reducing form errors with minimal support structures.* Journal of Manufacturing Systems, 2015. **36**: p. 231-243.

22. Jin, G.Q., W.D. Li, and L. Gao, *An adaptive process planning approach of rapid prototyping and manufacturing.* Robotics and Computer-Integrated Manufacturing, 2013. **29**(1): p. 23-38.

23. Habib, A., N. Ahsan, and B. Khoda, *Optimizing Material Deposition Direction for Functional Internal Architecture in Additive Manufacturing Processes.* Procedia Manufacturing, 2015. **1**: p. 378-392.

24. Jin, Y.-a., et al., *Optimization of tool-path generation for material extrusion-based additive manufacturing technology.* Additive Manufacturing, 2014. **1–4**: p. 32-47.

25. Ding, D., et al., *A tool-path generation strategy for wire and arc additive manufacturing.* International Journal of Advanced Manufacturing Technology, 2014. **73**(1-4): p. 173-183.

26. Huang, Y. and M.C. Leu, *Frontiers of Additive Manufacturing Research and Education: An NSF Additive Manufacturing Workshop Report*. 2014.

27. B. Huang, S.S., *Alternate slicing and deposition strategies for fused deposition modelling of light curved parts.* Journal of Acheivement in Materials nad Manufacturing Engineering, 2012. **55**(2): p. 511-517.

28. Khoda, A.K.M.B., I.T. Ozbolat, and B. Koc, *Engineered Tissue Scaffolds With Variational Porous Architecture.* Journal of Biomechanical Engineering, 2011. **133**(1): p. 011001.

29. O. S. Es-Said, J.F., R. Noorani, M. Mendelson, R. Marloth, *Effect of Layer Orientation on Mechanical Properties of Rapid Prototyped Samples.* Materials and Manufacturing Processes, 2000. **15**(1): p. 107-122.

30. Khoda, B., *Process Plan for Multimaterial Heterogeneous Object in Additive Manufacturing.* 3D Printing and Additive Manufacturing, 2014. **1**(4): p. 210-218.

31. Xu, F., H.T. Loh, and Y.S. Wong, *Considerations and selection of optimal orientation for different rapid prototyping systems.* Rapid Prototyping Journal, 1999. **5**(2): p. 54-60.

32. Singh, P. and D. Dutta, *Multi-Direction Slicing for Layered Manufacturing.* Journal of Computing and Information Science in Engineering, 2001. **1**(2): p. 129-142.

33. Dolenc, A. and I. Mäkelä, *Slicing procedures for layered manufacturing techniques.* Computer-Aided Design, 1994. **26**(2): p. 119-126.

34. Kim, H.-C. and S.-H. Lee, *Reduction of post-processing for stereolithography systems by fabrication-direction optimization.* Computer-Aided Design, 2005. **37**(7): p. 711-725.

35. Byun, H.S. and K.H. Lee *, *Determination of the optimal part orientation in layered manufacturing using a genetic algorithm.* International Journal of Production Research, 2005. **43**(13): p. 2709-2724.

36. Pham, D.T., S.S. Dimov, and R.S. Gault, *Part Orientation in Stereolithography.* The International Journal of Advanced Manufacturing Technology, 1999. **15**(9): p. 674-682.

37. Lan, P.-T., et al., *Determining fabrication orientations for rapid prototyping with Stereolithography apparatus.* Computer-Aided Design, 1997. **29**(1): p. 53-62.

38. Frank, D.a.F.G., *Expert system based selection of the preferred direction of build for rapid prototyping.* Journal of Intelligent Manufacturing, 1994. **6**: p. 334-339.

39. A.P. West, S.P.S., D.W. Rosen, *A process planning method to improve build performance in stereolithography.* Computer Aided Design, 2001. **33**: p. 65-79.

40. Lin F, S.W., Yan Y. , *Optimization with minimum process error for layered manufacturing fabrication.* Rapid Prototyping Journal, 2001. **7**(1).

41. Domingos, M., et al., *Evaluation of in vitro degradation of PCL scaffolds fabricated via BioExtrusion – Part 2: Influence of pore size and geometry.* Virtual and Physical Prototyping, 2011. **6**(3): p. 157-165.

42. Khoda, A.K.M.B. and B. Koc, *Functionally heterogeneous porous scaffold design for tissue engineering.* Computer-Aided Design, 2013. **45**(11): p. 1276-1293.

43. Khoda, A.K.M., I.T. Ozbolat, and B. Koc, *Designing heterogeneous porous tissue scaffolds for additive manufacturing processes.* Computer-Aided Design, 2013. **45**(12): p. 1507-1523.

44. Paul, R. and S. Anand, *Optimal part orientation in Rapid Manufacturing process for achieving geometric tolerances.* Journal of Manufacturing Systems, 2011. **30**(4): p. 214-222.

45. Frank, D. and G. Fadel, *Expert system-based selection of the preferred direction of build for rapid prototyping processes.* Journal of Intelligent Manufacturing, 1995. **6**(5): p. 339-345.

46. Jin, G.Q., et al., *A hybrid and adaptive tool-path generation approach of rapid prototyping and manufacturing for biomedical models.* Computers in Industry, 2013. **64**(3): p. 336-349.

47. See, T.-K., A. Gurnani, and K. Lewis, *Multi-Attribute Decision Making Using Hypothetical Equivalents and Inequivalents.* Journal of Mechanical Design, 2005. **126**(6): p. 950-958.

48. Habib, A., N. Ahsan, and B. Khoda. *Optimizing Material Deposition Direction for Functional Internal Architecture in Additive Manufacturing Processes (Accepted)*. in *43rd North American Manufacturing Research Conference*. 2015. Charlotte, NC.

49. Kim, B.H. and B.K. Choi, *Machining efficiency comparison direction-parallel tool path with contour-parallel tool path.* Computer-Aided Design, 2002. **34**(2): p. 89-95.

50. Watson, S.R. and A.N.S. Freeling, *Assessing Attribute Weights.* Omega, 1982. **10**(6): p. 582–583.

51. Weihua, S., et al. *Part geometric understanding for tool path planning in additive manufacturing*. in *Proceedings of the IEEE International Symposium onComputational Intelligence in Robotics and Automation*. 2003. Kobe, Japan.

52. Ultimaker. *CURA version 14.09*. [cited 2017 December]; Available from: https://ultimaker.com/en/products/cura-software/list.

53. Stratasys. *Insight version 5.1*. [cited 2015 December]; Available from: http://www.stratasys.com/3d-printers/design-series/fortus-250mc.

54. Montgomery, D.C., *Design and Analysis of Experiments*. 8 ed. 2012, NJ: Wiley.

55. Michalewicz, Z., *Genetic Algorithms + Data Structures = Evolution Programs*. 3rd, rev. and extended ed. 1996, New York: Springer-Verlag.

56. Goldberg, D.E., *Genetic Algorithms in Search, Optimization, and Machine Learning*. 1989, Reading, MA: Addison-Wesley.